Порфирины
Porphyrins

Макрогетероциклы
http://macroheterocycles.isuct.ru

Миниобзор
Microreview

Photoinduced Relaxation Processes in Self−Assembled Nanostructures: Multiporphyrin Complexes and Composites "CdSe/ZnS Quantum Dot−Porphyrin"

Eduard I. Zenkevich,[a@] and Christian von Borczyskowski[b]

[a]National Technical University of Belarus, Minsk 220013, Belarus
[b]Institute of Physics, Chemnitz University of Technology, Chemnitz, 09107, Germany
[@]Corresponding author E-mail: zenkev@tut.by

Here, we discuss self-assembled multicomponent organic/inorganic nanostructures. Self-assembled multiporphyrin triads were formed via non-covalent interactions of meso-phenyl bridged ZnOEP chemical dimer, $(ZnOEP)_2Ph$, with dipyridyl substituted tetrapyrrole extra-ligand. In tetrads, the dimer $(ZnOEP)_2Ph$ is covalently linked via 5-mesoposition to additional electron acceptors (quinone Q, pyromellitimide Pim). Using steady-state, time-resolved fluorescent and pump-probe results, main relaxation pathways have been elucidated: competing energy migration and photoinduced electron transfer (PET) in normal triads within ≤1.4 ps; very fast (within ~700 fs) PET in porphyrin triads containing pentafluorinated porphyrin remaining still efficient at 77-120 K; a bridge-dimer mediated long-range (r_{DA}=18-24 Å) superexchange PET "extra-ligand→Q or Pim" in tetrads. Self-assembly of nanostructures from semiconductor CdSe/ZnS quantum dots (QD) and tetra-meso-pyridyl- substituted porphyrins is also based on extra-ligation interactions and results in a strong quenching of QD photoluminescence (PL). At the same molar ratios $x =[H_2P(m-Pyr)_4]/[QD]$, the quenching is more effective for small QDs than for larger ones. From experimental Stern-Volmer PL quenching plots $I_0/I(x)$ and the quantum mechanical calculations for the electron wave functions it follows that the specificity of the exciton non-radiative decay in "QD-porphyrin" nanocomposites is due to the manifestation of inductive and mesomeric effects leading to the charge tunnelling through ZnS barrier in quantum confinement conditions.

Keywords: Multiporphyrin complexes, quantum dots, energy/electron transfer.

Introduction

Nanobiotechnology is a new frontier of research that combines two seemingly incompatible objects: the building blocks of life and synthetic structures, both of them at a tiny, molecular-sized level. Its focus is on the development of powerful techniques and methods that merge the strengths of nanotechnology, working typically in the range of 1 to 100 nanometers, and biophysics, to generate a new type of 'bio-nanomaterial' which has some uniquely designed properties. In this respect, the interest in emerging nanostructures (based on porphyrin macrocycles) is growing exponentially since they are not only good models for the mimicking the primary photoevents *in vivo* but also seem to be considered as promising building blocks for advanced multifunctional nanocomposites with potential applications in improved drug delivery systems, photodynamic therapy, nanovoltaic cells, optoelectronic memory, and highly efficient catalysts, among several others.[1-3] In fact, this direction is the supramolecular organic chemistry/photochemistry in solutions or at solid/liquid interfaces,[4] a highly interdisciplinary field of science covering the chemical, physical, and biological features of chemical species held together and organized by means of intermolecular binding interactions of various natures. The resulting crossover has provided novel principles and concepts in physico-chemistry such as molecular recognition, self-organization, regulation, cooperativity, replication and so

on. A significant interest of numerous scientific groups in this direction has been devoted to the design and investigation of tetrapyrrole compounds that fold or assemble predictably in order to form multicomponent well-defined arrays.[5-10] The second direction of nanotechnology is based on the preparation and characterization of colloidal semiconductor nanocrystals such as CdSe and other II-VI systems with pronounced quantum confinement effects and thus tuneable colour and redox properties.[11-14] Such nanocrystals become due to quantum size effects, quantum dots (QDs) and are often strongly emissive.[15] QD optical properties arise from several phenomena (viz. quantum confinement of charge carriers, surface effects, and geometrical confinement of photons) and have turned semiconductor nanocrystals into promising materials for many applications,[12,14,16] such as light-emitting diodes, lasers, charge-transfer composites, biology/medicine *etc*.

In this respect, the combination of the two directions, that is the anchoring of organic molecules to tuneable wide gap semiconductor colloidal nanocrystals, is of considerable scientific and practical interest.[17-23] In heterocomposites of this type, the phenomena of photosensitized electron injection from organic subunits to semiconductor nanoparticles is used to activate charge separation with visible light quanta less than the semiconductor band gap energy.[17] In addition, non-radiative energy transfer depending on absorption/emission properties and intercenter distances between

coupled interacting nanoparticles-dye moieties strongly influences the dynamics and relaxation pathways in such complex systems.[18-19,21-23] The other driving force for the growing interest in the heterocomposites is due to the use of QD as photoluminescence markers linked to biological relevant molecules[24] and the creation of new optical and laser materials.[25,26]

With all these ideas in mind, we have developed a concept to self-assemble biomimetic porphyrin arrays which are tuneable with respect to photoinduced energy/electron transfer and charge separation. The key-hole organization principle is based on the complexation of central Zn ions of porphyrin chemical dimers or trimers with suitable extra-ligands (di- and tetrapyridyl substituted tetrapyrrolic macrocycles) *via* two-fold non-covalent coordination.[6,27] It was shown that the complexation is essentially based on a "Lego-type" key-hole principle effectively controllable *via* steric factors such as distance matching, optimization of relative orientations and solvent compositions. Recently, as an approach towards large-scale nanoassemblies we have successfully extended the above principle for the directed passivation of CdSe/ZnS core/shell QD surface by pyridyl-substituted tetrapyrrolic organic ligands.[19-21] We could prove the complexation of the molecules to the surface by steady-state titration and time-resolved fluorescence measurements.

In this review paper, we discuss our results on structural and photophysical properties of self-assembled multiporphyrin complexes as well CdSe/ZnS QDs upon their competitive interaction with tetrapyridyl substituted porphyrin extra-ligands showing that the principles of organic supramolecular chemistry may be appropriately employed to form a variety of "QD-organics" nanocomposites that are capable for possible applications.

Experimental

Self-Assembled Triads and Tetrads with Participation of Tetrapyrrolic Macrocycles

Details of the precursor molecular blocks preparation (Zn-octaethylporphyrin chemical dimers with a *meso*-phenyl spacer, (ZnOEP)₂Ph; pyridyl containing porphyrin extra-ligands), the formation of multiporphyrin complexes as well as experimental technique have been reported earlier.[6, 27-29] Typically, at ambient temperature multiporphyrin complexes of various structure and composition are formed during a titration of the chemical dimer (ZnOEP)₂Ph solution by the extra-ligand solution or by one-step mixing of the two solutions at appropriate concentrations. In the case of pair interactions, complexation constants K_C for the triad formation have been obtained by the conventional technique[28] on the basis of both absorption and fluorescence data measured in the titration experiments using the following expression:

$$K_C = (1 - \beta) \cdot \frac{1}{C_{D0} \cdot \beta (x + \beta - 1)} \tag{1}$$

where C_{D0} is the initial concentration of dimer (ZnOEP)₂Ph, $x = $ [ligand]/[(ZnOEP)₂Ph] is a molar ratio with [ligand] as the total experimental concentration of the extra-ligand in the solution; $\beta = I/I_0$ is the portion of the uncomplexed dimer molecules which can be estimated from the fluorescence of the uncomplexed dimer;
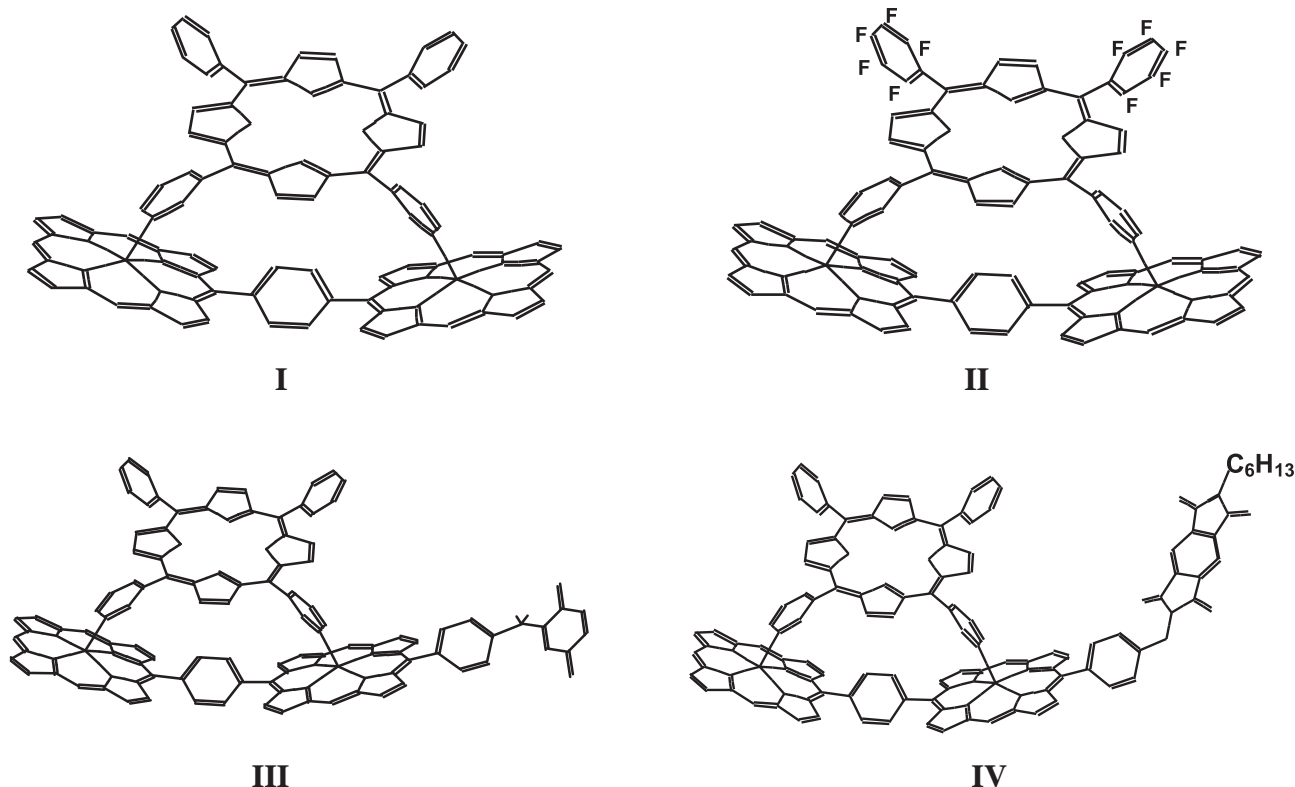

I

II

III

IV

Chart 1. Mutual arrangement of chemical dimer (ZnOEP)₂Ph, porphyrin extra-ligands in triads (**I, II**) and tetrads (**III, IV**) containing electron acceptors, quinone (Q) and piromellitimide (Pim). Optimised geometries were calculated on the basis of HyperChem software package (release 4, semiempirical method PM3). For clarity, side alkyl substituents in pyrrole rings of the dimer and mesophenyl rings of the extra-ligand are omitted. **I**: (ZnOEP)₂Ph⊗H₂P(m^Pyr)₂-(*iso*-PrPh)₂; **II**: (ZnOEP)₂Ph⊗H₂P(m^Pyr)₂-(5FPh)₂; **III**: (ZnOEP)₂Ph-Q⊗H₂P(m^Pyr)₂-(*iso*-PrPh)₂; **IV**: (ZnOEP)₂Ph-Pim⊗H₂P(m^Pyr)₂-(*iso*-PrPh)₂.

I and I_0 are the measured and initial integral fluorescence intensities of the uncomplexed dimer in the titration solution, respectively. Due to the two-fold extra-coordination, complexation constants for self-assembled triads with participation of dimer $(ZnOEP)_2Ph$ and $H_2P(Pyr)_n$ were estimated to be $K_C \sim 5\times10^6$ M^{-1} - 2×10^7 M^{-1} (depending on the position of *meso*-pyridyl rings, opposite or adjacent) and are of two or three orders of magnitude larger than those obtained for the di-pyridinated dimer $(ZnOEP)_2Ph$.[6,27-29] It means that the multiporphyrin systems under study are characterized by strong allosteric behaviour showing that the first binding accelerates the second binding because of the chelate effect. Two types of the triads with the same geometry will be discussed below: the triad with porphyrin extra-ligand $H_2P(m^\wedge Pyr)_2$-(*iso*-PrPh)$_2$ and the other one having 5,10-di(pentafluorophenyl)-15,20-dipyridyl free base porphyrin, $H_2P(m^\wedge Pyr)_2$-(5FPh)$_2$ known as a strong electron acceptor.[29,30] In addition, the chemical dimer $(ZnOEP)_2Ph$ may be covalently linked in *meso*-position to an electron acceptor *p*-benzoquinone (Q) or pyromellitimide (Pim), having different redox properties and fixed at the same distance and geometry with respect to the dimer.[30] Correspondingly, in such tetrads, we like to concentrate on some aspects of interporphyrin and porphyrin-quinone photoinduced electron transfer competing with the non-radiative electronic excitation energy transfer. The structures of the corresponding self-assembled triads and tetrads are shown in Chart 1.

"CdSe/ZnS Quantum Dot−Porphyrin" Nanocomposites

The n-trioctylphosphine oxide (TOPO) caped highly monodisperse CdSe nanocrystals (or quantum dots, QD) with an inorganic ZnS shell were used in order to form semiconductor QD-porphyrin heterostructures in toluene (or chloroform) at ambient temperature. Taking into account the existence of an inorganic ZnS shell covering CdSe QDs we have succeeded to realize the surface passivation of CdSe/ZnS QDs by *meso*-pyridyl substituted porphyrins using the self-aggregation approach described above for multiporphyrin arrays (replacing Zn-porphyrin dimers with QDs).[19,20] The colloidal TOPO-capped core/shell CdSe/ZnS quantum dots were obtained from Evident Technologies, Inc, Troy, NY, USA. The diameters d_{CdSe} of QD vary between 2.1 and 5.2 nm, while–in most cases–two capping ZnS monolayers have been applied. The absorbance of the QD starting solutions was adjusted

to be lower than 0.1 OD at excitation and emission wavelengths in order to avoid non-linear absorption and re-absorption effects. The concentrations varied in the range $(1\div10)\times10^{-7}$ M. Stability and purity of the QD solutions were checked by measuring the quantum yield stability at least over 3 hrs after preparation. Titration experiments were carried out by adding $H_2P(m\text{-}Pyr)_4$ to the QD solution at relative molar ratios $x = [porphyrin]/[QD]$ in toluene, thus varying the number of porphyrin molecules on the QD surface. Details on the material properties and experimental setup are presented in our recent publications.[31,32] Figure 1 shows a schematic presentation of such a hetero nanoassembly consisting of a QD with the tri-*n*-octyl phosphine oxide (TOPO) surfactant layer and one $(m\text{-}Pyr)_4$-H_2P molecule attached via its meso-pyridyl rings nearly perpendicular to the QD surface.

At ambient temperature, the titration of CdSe/ZnS QD toluene solution by a comparable amount of meso-pyridyl substituted porphyrin molecules $H_2P(Pyr)_n$ manifests itself in the QD photoluminescence (PL) quenching (the relative intensity decrease and decay shortening[19,20,31,32]). This has been interpreted as being due to the formation of nanoassemblies *via* anchoring porphyrin ligating molecules on the ZnS surface. It has been shown that the quenching efficiency and thus the probability to form "QD-porphyrin" complex scales with the number of pyridyl rings having access to the QD surfaces, being the strongest one in the case of tetra-pyridyl substituted porphyrin $H_2P(Pyr)_4$. Like for porphyrin self-assembled triads, the importance of the designed two-point interacting domain has been also demonstrated upon formation of the CdSe/ZnS QD-porphyrin nanocomposites. Here, we will discuss physico-chemical properties of such nanocomposites based on QDs of various sizes and $H_2P(Pyr)_4$ molecules.

Results and Discussion

Excited States Properties and Relaxation Dynamics in Triads I and II

Typically, for porphyrin triads $(ZnOEP)Ph_2\otimes H_2P(m^\wedge Pyr)_2$-(*iso*-PrPh)$_2$ (type **I**, Chart 1) and $(ZnOEP)_2Ph\otimes H_2P(m^\wedge Pyr)_2$-(5FPh)$_2$ (type **II**, Chart 1) of the same geometry visible absorption bands of the dimer $(ZnOEP)_2Ph$ are shifted to the red ($\Delta\nu\sim450$ cm^{-1}) with the essential intensity redistribution in comparison with those for

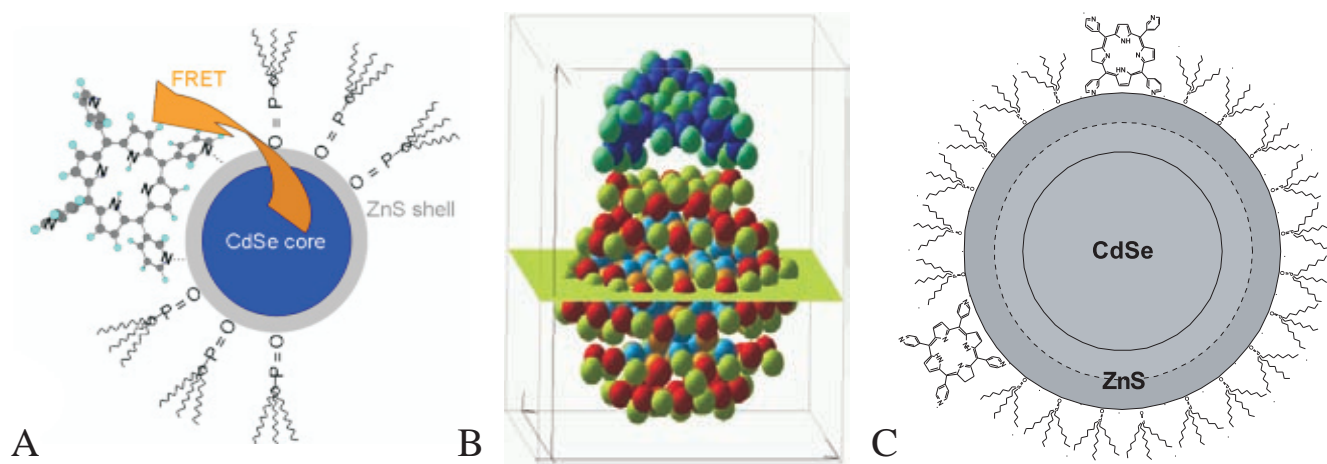**Figure 1**. Schematic presentation of "QD-porphyrin" nanostructures (A), an optimized geometry for $Cd_{33}Se_{33} + H_2P(m^\wedge Pyr)_2$ (B, optimisation by HyperChem 7.0; simulations by *ab initio* density functional theory, DFT, with the VASP code [21]) and the scales of CdSe core, ZnS shell, porphyrin and TOPO molecules corresponding to relative sizes of the main components of the arrays (C): the ZnS shell thickness for QDs was estimated on the basis of the thickness of one ZnS layer l = 5 Å; parameters for conical TOPO molecules r_{bottom} = 5.5 Å, h_{con} = 9.9Å; r_m = 7.5Å is the radius of porphyrin molecule with opposite pyridyl rings having nitrogens in meta-positions, h = 10 Å is the mean distance between meta-nitrogens of adjacent pyridyl rings (HyperChem 4.0, semiempirical method PM3).
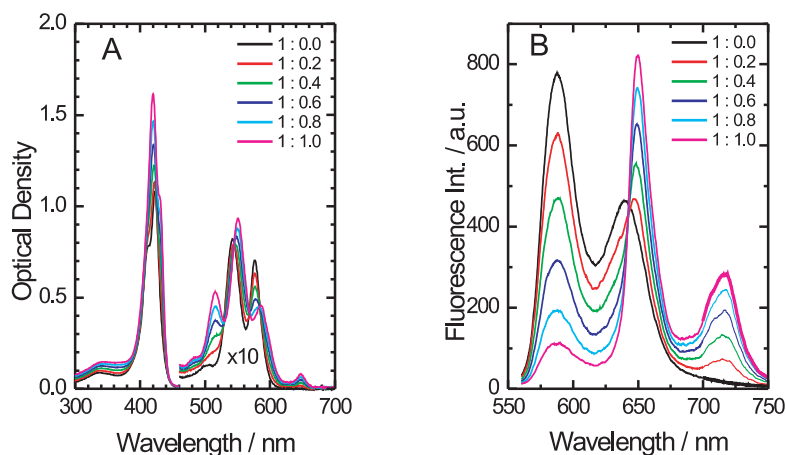
Figure 2. Absorption (A) and fluorescence (B, λ_{ex}=546 nm, isosbestic point) spectra of the dimer (ZnOEP)$_2$Ph with increasing amounts of extra-ligand H$_2$P(m^Pyr)$_2$-(*iso*-PrPh)$_2$ (toluene, 295 K). Concentration of (ZnOEP)$_2$Ph at the beginning of titration is C_{D0}=1.9·10^{-6} M. The ligand:dimer molar ratio varies from x=0.0 to 1.0 (0.0, 0.2, 0.4, 0.6, 0.8, 1.0). The low-intense unshifted fluorescence band at λ_{max}=586 nm in triad solution at x= 1:1 belongs to the remaining uncompleted dimer.

the individual dimer (Figure 2A).[6,27,28] These observations are very similar to the effects taking place for complexes of Zn-porphyrins and their chemical dimers with pyridine or pyridyl-containing molecules.[33] Absorption spectra of both triads are a linear combination of the corresponding di-pyridinated dimer (ZnOEP)$_2$Ph and the corresponding porphyrin extra-ligand, with only small differences in wavelength maxima and band shapes. Thus, the interaction

between the two subunits is weak in the ground state, and they retain their individual identities.

In both triads, the dimer fluorescence does show strong quenching (fluorescence decay is shorten from τ_{SD}^0=1.15 ns down to $\tau_{SD} \leq$ 1.7 ps for the triad **I** in toluene at 295 K [29]), and fluorescence spectra of the triads mainly consist of the porphyrin extra-ligand fluorescence bands (Figure 2B). Main fluorescent features in the triad of type **I**, (ZnOEP)$_2$Ph⊗H$_2$P(m^Pyr)$_2$-(*iso*-PrPh)$_2$, are as follows (Figure 3). 1) In nonpolar toluene at 295 K, the extra-ligand fluorescence quantum efficiency is reduced by 1.5-2 times as compared to the individual H$_2$P(m^Pyr)$_2$-(*iso*-PrPh)$_2$. 2) The extra-ligand fluorescence intensity is decreased upon temperature lowering (278-160 K). 3) The increase of the solvent polarity by a subsequent acetone addition to toluene leads to the decrease of the extra-ligand fluorescence intensity (bands at 650 nm and 714 nm) while the fluorescence of the individual extra-ligand does not show fluorescence quenching upon acetone addition. 4) At 295 K in toluene, fluorescence excitation spectrum of the triad **I** detected at extra-ligand fluorescence bands ($\lambda_{det} \geq$720 nm, toluene, 293 K) clearly shows the existence of absorption bands of the dimer (549 nm and 587 nm), while upon addition of 17 vol% of acetone admixture in toluene the dimer emission in the triad remains strongly quenched but the form of the excitation spectrum of the triad becomes almost identical to that of the individual extra-ligand H$_2$P(m^Pyr)$_2$-(*iso*-PrPh)$_2$.

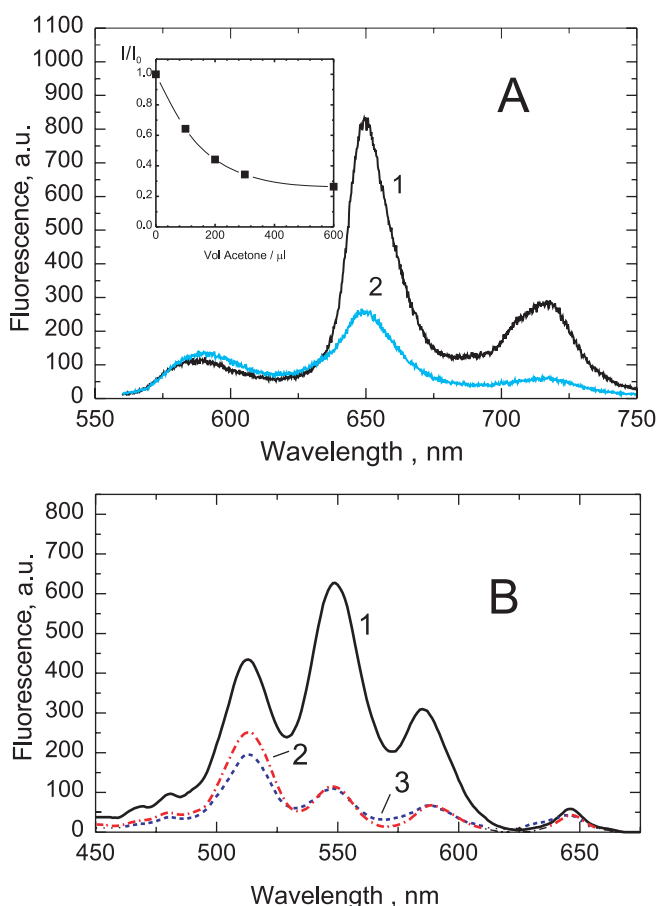**Figure 3.** Fluorescence (A, λ_{ex}=546 nm) and fluorescence excitation spectra (B, λ_{em}=720 nm) of the triad (ZnOEP)$_2$Ph⊗H$_2$P(m^Pyr)$_2$-(*iso*-PrPh)$_2$ in toluene (1) and toluene+17 vol% of acetone solutions at 295 K (2). Curve 3B corresponds to fluorescence excitation spectrum (λ_{em}=720 nm) of individual H$_2$P(m^Pyr)$_2$-(*iso*-PrPh)$_2$. Insert: dependence of the extra-ligand fluorescence intensity in the triad (λ_{ex}=650 nm) on acetone admixture.
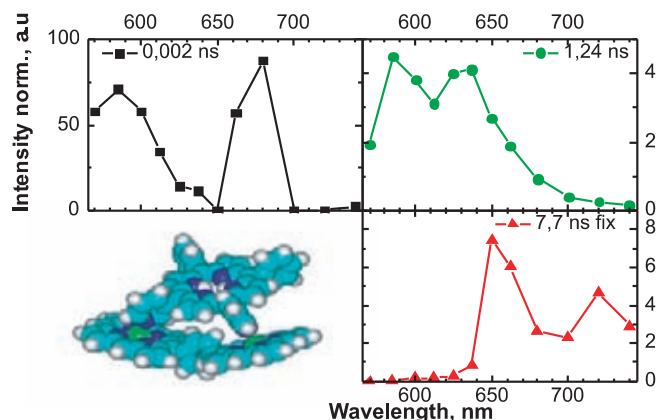

Figure 4. Decay-associated spectra of the triad (ZnOEP)$_2$Ph⊗H$_2$P(m^Pyr)$_2$-(*iso*-PrPh)$_2$ (toluene, 293 K, λ_{ex} = 546 nm) derived from a global analysis of 12 time correlated single photon counting (TCSPC) fluorescence measurements. The global χ^2 value was 1.15.

It indicates that the sensitization effect due to the singlet-singlet energy migration (S-S EM) process is absent, though usually through-space S-S EM process in multiporphyrin arrays is hardly dependent on the solvent polarity.[35] At last, the analysis of the excited-state dynamics in the triad **I** using time correlated single photon counting (TCSPC) fluorescence measurements (Figure 4) and a global fit procedure with three time constants[35] shows that the fluorescence decays of extra-ligand in the triads are reduced noticeably with respect to those for individual uncomplexed porphyrin. The decay time shortening increases upon the solvent polarity rise (τ_S=5.5 ns for $H_2P(m\text{^}Pyr)_2$-(iso-PrPh)$_2$ in the triad in toluene + 7 vol% of acetone), the last tendency correlates with a pronounced decrease of the extra-ligand fluorescence quantum yield. Femtosecond pump-probe data obtained for the triad $(ZnOEP)_2Ph \otimes H_2P(m\text{^}Pyr)_2$-($iso$-PrPh)$_2$ in toluene at 295 K reveal[29] that the non-radiative relaxation of the dimer S_1-state in the triads realizes within ~1.7 ps.

In the result, on the basis of the detailed experimental data in the combination with theoretical calculations the whole scheme of the dynamics of locally excited S_1-states for components in triad **I** has been evaluated[34,36,37] as follows (Figure 5). The non-radiative deactivation of the dimer locally excited S_1-state is caused by competing S-S-EM and photoinduced electron transfer PET processes (Figure 5, rate constants k_5 and k_6). The competition between S-S-EET and PET channels depends on photophysical and redox parameters of the subunits and may be driven by temperature and polarity of surrounding. Applying Foerster inductive-resonant model[38] to the triads with known geometrical, spectral and kinetic parameters (intercenter dipole-dipole distance r_{DA}=8.8 Å, orientation factors k^2=0.75, fluorescence lifetime τ_S^0=1.15 ns, quantum yield φ_S=0.012 for dipyridinated $(ZnOEP)_2Ph$, toluene, 293 K) we calculated spectral overlap integrals
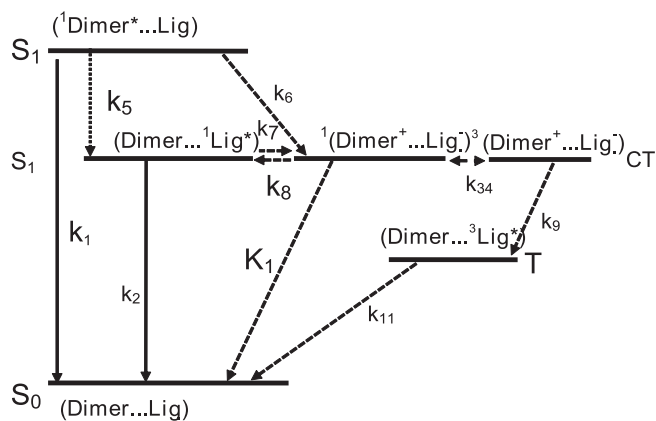
$$J = \int_0^\infty f_D(v)\varepsilon_A(v)\frac{dv}{v^4} = 4.2 \cdot 10^{-14} \text{ cm}^{-3} \cdot \text{M}^{-1} \text{ and critical}$$

transfer distances R_0^{theor} =20.3 Å. Thus, theoretical value of S-S EM rate constant is $k_5 = k_{EM} = (1/\tau_S)(R_0^{theor}/r_{DA})^6 = 1.37 \cdot 10^{11}$ s^{-1}, and the dimer S_1-state decay has to be decreased to values of ~7÷8 ps due to S-S EM only. In this respect, the observed stronger shortening of the dimer $(ZnOEP)_2Ph$ S_1-state decays in the triad **I** (toluene, 295 K) is most likely attributed to a Foerster type EM and an additional competing PET process. This quenching is followed by the population of the locally excited S_1-state of the extra-ligand via S-S EM with a rate constant k_5 and the formation of the radical ion pair singlet state via PET process with a rate constant k_6 (Figure 5).

Our theoretical results[36,37] have shown that the generalized Haken-Strobl-Reineker formalism provides both qualitative and quantitative description of time-resolved and steady-state properties such as fluorescence quenching in triads of type **I** due to competing PET and EM processes. From the theoretical point of view coherent or incoherent type of electron or exciton transport in the systems under consideration depends on the coupling to the relevant vibrational modes. Table 1 collects structural, photophysical and photoinduced electron transfer parameters for triad **I** being used in calculations.

It is seen from Table 1 that charge transfer (CT) state for the photoinduced electron transfer $(ZnOEP)_2Ph \rightarrow$ extra-ligand are very close with locally excited $\tilde{S}_1$-states of the extra-ligand. This situation explains the existence of stimulated fluorescence of the extra-ligand in pure toluene at 295 K (Figure 3, curve 1B) as a result of simultaneous realisation of S-S EET, EM and repopulation processes. The increase of the solvent polarity (addition of acetone) leading to CT state lowering manifests itself in the extra-ligand fluorescence additional quenching and the absence of sensitising effect, which may hint to ET process presumably involved in the later case. It should be mentioned also that the photoinduced hole transfer from the excited state of the extra-ligand (Dimer...^{1}Lig*) to the dimer (rate constant k_7) may lead to the singlet radical ion pair state formation ^{1}(Dimer$^+$...

Figure 5. Schematic energy diagram for locally excited singlet states of the dimer $(ZnOEP)_2Ph$ {S_1,(^{1}Dimer*...Lig)}, the extra-ligand H_2P {S_1,(Dimer...^{1}Lig*)}, locally excited triplet state of H_2P {T_1 (Dimer...^{3}Lig*)}, radical ion pair singlet {^{1}(Dimer$^+$...Lig$^-$)} and triplet {^{3}(Dimer$^+$...Lig$^-$)} states. Indicated are rate constants of the following pathways: k_1, fluorescence and non-radiative decay of the dimer; k_2, fluorescence and non-radiative decay of the extra-ligand; k_5, singlet-singlet EM $(ZnOEP)_2Ph \rightarrow H_2P$; k_6, photoinduced electron tran-sfer (PET) $(ZnOEP)_2Ph \rightarrow H_2P$; k_7, photoinduced hole transfer $H_2P \rightarrow (ZnOEP)_2Ph$; k_8, thermally acti-vated charge recombination; k_{34}, spin rephasing in radical ion pair; k_9, charge recombination of the triplet radical ion pair; k_{10}, charge recombination of the singlet radical ion pair to the ground state; k_{11}, H_2P non-radiative intersystem crossing $T_1 \rightsquigarrow \rightsquigarrow S_0$.

Table 1. Structural, photophysical and photoinduced electron transfer parameters for the triad $(ZnOEP)_2Ph \otimes H_2P(m\text{^}Pyr)_2$-($iso$-PrPh)$_2$ (toluene, 295 K).

r_{DA} Å	E_A^{red} eV	$E(S_1^D)$ eV	$E(IP)$ eV	τ_{S0}^{Dim} ns	τ_{S0}^L ns	τ_S^L ns
8.8	-1.01	1.91	1.90	1.15	9.5	7.7

Intercenter distances r_{DA} were estimated from optimised structures of the triads (HyperChem software package, release 4, semiempirical method PM3). The oxidation potential for coordinated dimer $(ZnOEP)_2Ph$ was taken to be $E_{1/2}^{ox}$=0.63 V, reduction potential E_A^{red} for extra-ligand has been extracted from literature data. The energy levels of the ion pair states in toluene were calculated by $E(IP) =$

$$= e(E_D^{ox} - E_A^{red}) + \frac{e^2}{4\pi\varepsilon_0}\left[\left(\frac{1}{2r_D} + \frac{1}{2r_A} - \frac{1}{r_{DA}}\right)\frac{1}{\varepsilon} - \left(\frac{1}{2r_D}\frac{1}{\varepsilon_D'} + \frac{1}{2r_A}\frac{1}{\varepsilon_A'}\right)\right]$$

(details of calculations are presented in our earlier papers.[6, 34, 36, 37] τ_{S0}^{Dim} is measured fluorescence decay for individual dimer in toluene+pyridine, τ_{S0}^L and τ_S^L are measured fluorescence decays for the individual extra-ligand and in the triad, correspondingly.

Lig⁻). In its turn, the fast repopulation of the extra-ligand S_1-state is caused by the effective thermally activated charge recombination (rate constant k_8) from the singlet radical ion pair state ^{1}(Dimer⁺...Lig⁻) to the close-lying locally excited singlet state (Dimer...^{1}Lig*). At last, the repopulation of the extra-ligand S_1-state may take place also via the following sequence (Figure 5).

$$(^1\text{Dimer}^*...\text{Lig}) \xrightarrow{k_6} (\text{Dimer}^+...\text{Lig}^-) \xrightarrow{k_8}$$
$$\xrightarrow{k_8} (\text{Dimer}...^1\text{Lig}^*)$$
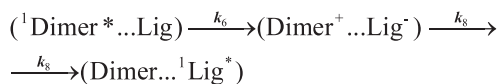
At last, we have shown for the triads of type **I**,[6,33,34] that the direct intersystem crossing $S_1 \leadsto T_1$ in the extra-ligand subunit is extremely low in comparison with the processes discussed above. The population of the extra-ligand locally excited T_1-state may take place from the upper lying triplet radical ion pair state ^{3}(Dimer⁺... Lig⁻) formed via the spin rephasing between the singlet and triplet radical ion pairs (rate constant k_{34}, Figure 5).

In reality, experimental results evidently show that the dynamics of electronic excitation energy deactivation in triads **I** and **II** is not the same.[34] While the absorption spectra of the titration experiments for the dimer (ZnOEP)Ph₂ with H₂P(m^Pyr)₂-(*iso*-PrPh)₂ and H₂P(m^Pyr)₂-(5FPh)₂ ligands are very similar but great differences are observed in fluorescence spectra of the triad **II** in comparison to the triad **I**. It is seen from Figure 3A that for the triad **I** the fluorescence of the non-fluorinated extra-ligand H₂P(m^Pyr)₂-(*iso*-PrPh)₂ (with bands at 650 and 716 nm) increases with increasing concentration of this ligand. In contrast, for the triad **II** almost no fluorescence of the fluorinated extra-ligand H₂P(m^Pyr)₂-(5FPh)₂ is observed.[34] So, the striking difference between triads **I** and **II** is the pronounced quenching of the free base fluorescence for the triad **II**. Although the emission of this extra-ligand is very weak in the triad **II** fluorescence spectra and fluorescence

excitation spectrum (monitored at 717 nm where the major part of fluorescence is from the extra-ligand) can still be observed (with appropriate signal amplification). At 295 K in toluene, with respect to the fluorescence excitation spectrum of the triad **I** (clearly showing the existence of absorption bands of the dimer 549 nm and 587 nm, curve 1 in Figure 3B), the triad **II** shows completely different behavior. The excitation spectrum in the last case is identical in shape to that of the individual H₂P(m^Pyr)₂-(5FPh)₂, indicating, that no fluorescence is sensitized via (ZnOEP)Ph₂ absorption. In fact, the rest small emission in solution with the triad **II** can be attributed completely to non-bound extra-ligand).

Femtosecond pump-probe measurements give a dipper insight in the electronic excitation energy dynamics for the triad **II**.[34,37] Time resolved spectra are presented in Figure 6. The main features which can be recognized are ground state bleaching of the porphyrin Q-bands at 515, 550 and 580 nm and a broad absorption at around 670 nm (Figure 6A). From the steady-state absorption spectra the band at 515 nm can be assigned to the free base absorption while those at 550 and 580 nm are mainly determined by the dimer (ZnOEP)Ph₂. Absorption at 670 nm is usually ascribed to the Zn-porphyrin cation.[39] The transients of the absorption at 510 nm and 670 nm are shown in Figure 6B. At λ_{rec}=510 nm the optical density (OD) decreases after an immediate rise at time zero. The decay was fitted with time constant 0.7 ($\pm$0.1) ps. At λ_{rec}=670 nm an immediate rise of the OD is observed in accord with the time constant of 0.7 ps found for the 510 nm decay. A similar transient (data not shown) could be found at 890 nm where anion [H₂P(m^Pyr)₂-(5FPh)₂]⁻ is expected to absorb.[40]

These data indicate that for the triad **II** an extremely fast PET takes place on a time scale of 0.7 ps. (free Gibbs energy $\Delta G^0 \approx -0.25$eV, energy of charge transfer state E(IP) = 1.66 eV, r_{DA}=8.8 Å).[29] No fluorescence is sensitized via the dimer absorption, and correspondingly S-S energy migration (ZnOEP)₂Ph*→H₂P(m^Pyr)₂-(5FPh)₂ is not realized at 295
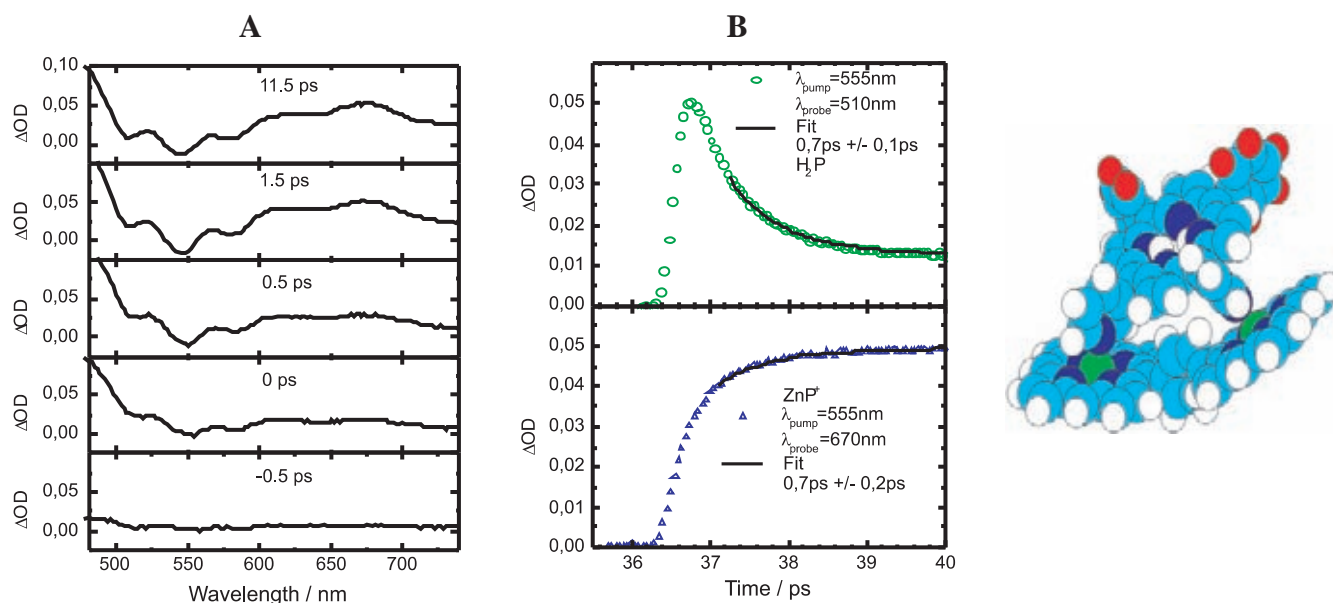

Figure 6. Femtosecond pump-probe data for the triad **II** (ZnOEP)₂Ph⊗ H₂P(m^Pyr)₂-(5FPh)₂ with fluorinated extra-ligand in toluene at 295 K: **A** - Time-resolved transient absorption spectra at various delay times with respect to the exciting pump pulse at 400 nm. **B** - Time evolution of the transient absorbance for the fluorinated triad formed by the excitation at 555 nm and measured at 510 nm (top) and 670 nm (bottom).

K. In rigid glassy matrices and PMMA thin films at 120-77 K this photoinduced ET remains still effective (rate constant is $k_{PET} \sim 10^{11} s^{-1}$) and competes with the singlet-singlet EM process from the dimer to the extra-ligand.[29] Some reasons for the effective low-temperature ET in this case may be considered i) The fluorinated porphyrin free base is strongly electron withdrawing and stabilizes a negative charge on its π-conjugated macrocycle; ii) The coordination of the electron-donating pyridyl rings helps to stabilize a positive charge on the Zn-dimer and thus lowers the energy of the radical ion pair state ^{1}(Dimer$^+$...Lig$^-$). In the triad **II** PET is adiabatic at room temperature, while in rigid solution at 77 K electron quantum tunneling may take place.

Because of fast PET in the triad **II** the direct population of the locally excited triplet T_1-state of the fluorinated extra-ligand can take place via intersystem crossing. In this case, the effective formation of the extra-ligand low lying T_1-state (τ_T=6.4μs in degassed solution) takes place from the upper-lying triplet or singlet radical ion pair states. Finally, it should be noted that PET processes in many biological objects (including photosynthetic reaction centers[3]) appear to be operative at cryogenic temperatures, while only few model systems[41] with this property (including our discussed here) have been described.

Pathways and Dynamics of Relaxation Processes in Tetrads III and VI with Covalently Linked Electron Acceptors

Using two the distance-fixed dimers with the same spacers but containing different electron acceptors of non-porphyrin nature, namely quinone (ZnOEP)$_2$Ph-Q, and pyromellitimide (ZnOEP)$_2$Ph-Pim we have formed self-assembled tetrads (ZnOEP)$_2$Ph-Q⊗H$_2$P(m-Pyr)$_2$-(*iso*-PrPh)$_2$ (tetrad **III**) and (ZnOEP)$_2$Ph-Pim⊗H$_2$P(m^Pyr)$_2$-(*iso*-PrPh)$_2$ (tetrad **IV**), characterized by the same geometry with respect to triads **I** and **II** with the same geometries (Chart 1).[6,30,34] Noteworthy, absorption spectra of tetrads **III** and **IV** do practically not differ from those obtained for triads **I** or **II**. This implies that in *A*-containing tetrads porphyrin chromophores act as entirely independent light absorbing entities. Titration experiments indicate also that fluorescence spectra of *A*-containing tetrads are characterized by a substantial quenching of the dimer (ZnOEP)$_2$Ph fluorescence. Therefore in all cases the fluorescence spectra of the tetrads **III** and **IV** mainly consist of the free-base extra-ligand H$_2$P(m^Pyr)$_2$-(*iso*-PrPh)$_2$ fluorescence bands. This important observation implies that the fluorescence of the covalently linked systems (ZnOEP)$_2$Ph-Q and (ZnOEP)$_2$Ph-Pim already being strongly quenched due to PET process from the dimer to *A*,[6,34] does show a remarkable additional quenching upon the tetrad formation in toluene at 295 K. The second feature observed for tetrads with covalently linked acceptors is that the fluorescence quantum efficiencies (φ$_F$) of the extra-ligand in tetrads are essentially smaller as compared not only to individual extra-ligand H$_2$P(m^Pyr)$_2$-(*iso*-PrPh)$_2$ but also to the same extra-ligand in the corresponding triad **I** without *A*. The decrease of φ$_F$ values is more pronounced for the Q-containing tetrad **III** as compared to the Pim-containing tetrad **IV**. At last, the analysis of fluorescence excitation spectra (λ_{det} =720 nm) measured for tetrads **III** and **IV** at
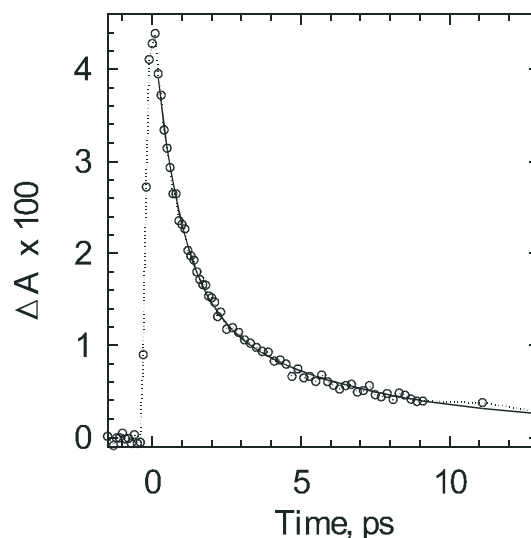

Figure 7. Time evolution of the transient absorbance for the tetrad **IV** (ZnOEP)$_2$Ph-Pim⊗H$_2$P(m^Pyr)$_2$-(*iso*-PrPh)$_2$ in toluene at 295 K (λ_{pump}=555 nm - in the dimer absorption band, λ_{probe}= 515 nm - the region of the extra-ligand ground state bleaching cased by the formation of H$_2$P* and H$_2$P$^-$ species). Two-exponential fit I(t)=A$_1$·exp(-t)+A$_2$·exp(-t/τ_2)+δ(t) gives τ_1=0.9 ps (A$_1$=0.029) and τ_2=5.4 ps (A$_2$= 0.015).

295 K in pure toluene and upon acetone addition (9 vol%) leads to the conclusion that in these systems S-S EM process (ZnOEP)$_2$Ph*→H$_2$P(m-Pyr)$_2$-(*iso*-PrPh)$_2$ is slow compared to other pathways (including PET) of electronic energy deactivation of the S$_1$-excited dimer.

Femtosecond pump-probe results reveal the faster complex non-radiative excited state behaviour being observed within τ_1=0.7-7.0 ps for tetrads **III** and **IV** (in toluene at 295 K (Figure 7) The detailed analysis of femtosecond spectral-kinetic data shows that the formation of CT states could be appropriately detected.[6, 34]

To get a more quantitative insight into the dynamics of relaxation processes in the systems under consideration the fluorescence decay times of the *A*-containing tetrads were evaluated using TCSPC measurements (λ_{ex}=546 nm, detection range of 570 nm - 750 nm, the longest time component belonging to the corresponding uncomplexed extra-ligand was fixed[34]). Time-amplitude spectra are shown in Figure 8 and Table 2 lists the evaluated fluorescence decay times for the complexed extra-ligands in tetrads **III** and **IV**. As was discussed in previous section, a small but noticeable shortening of fluorescence decays were detected for the same extra-ligand H$_2$P(m-Pyr)$_2$-(*iso*-PrPh)$_2$ in triad **I** without *A* (Table 1) that have been attributed to a photo-induced hole transfer from the extra-ligand to the dimer. Comparison of data collected in Tables 1 and 2 indicate an essential shortening of fluorescence decays for the extra-ligand in *A*-containing tetrads **III** and **IV** with respect to that found for the triad **I** without *A*. In fact, TCSPC data reflect the final steps of the electronic energy excitation dynamics in *A*-containing tetrads.

As was discussed in previous section in toluene at 295 K for the triad **I**, a noticeable shortening of the extra-ligand H$_2$P(m^Pyr)$_2$-(*iso*-PrPh)$_2$ fluorescence decay is due to the photoinduced hole transfer from the excited state of the extra-ligand (Dimer...^{1}Lig*) to the dimer (rate constant

Table 2. Measured and estimated values for superexchange PET in A-containing tetrads **III** and **IV** (toluene, 295 K).

Tetrad	Donor	Bridge	A	$E(S_1^D)$ eV	r_{DB} Å	r_{DA} Å	E_D^{OX} eV	$E_{D^+B^-A}$ eV	τ_{S0}^L ns	τ_S^L ns	k_{PET}, 10^8 s^{-1}
III	$H_2P(m\text{-}Pyr)_2\text{-}(iso\text{-}PrPh)_2$	$(ZnOEP)_2Ph$	Q	1.91	8.2	18.0	1.10	3.08	7.7	0.94	9.9
IV	$H_2P(m^\wedge Pyr)_2\text{-}(iso\text{-}PrPh)_2$	$(ZnOEP)_2Ph$	Pim	1.91	9.1	24.2	1.10	3.08	7.7	2.67	3.6

Rate constants for bridge-mediated superexchange PET were calculated by $k_{PET} = (\tau_S^L)^{-1} - (\tau_{S0}^L)^{-1}$.
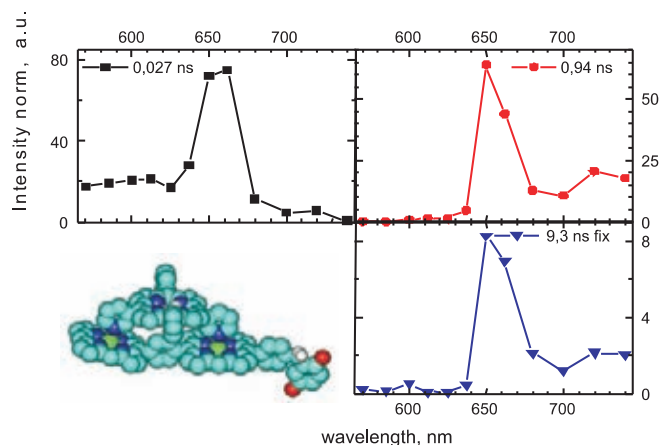
Figure 8. Decay-associated spectra of the tetrad **III** (toluene, 295 K, λ_{ex} = 546 nm) derived from global analysis of 12 TCSPC time-resolved fluorescence measurements.

k_7, Figure 5) leading to the singlet radical ion pair state formation $^1(Dimer^+...Lig^-)$. The corresponding rate constant is estimated to be $k_{HT} = (\tau_S^L)^{-1} - (\tau_{S0}^L)^{-1} = 2.3 \cdot 10^7$ s^{-1}. In contrast for example for Q-containing tetrad **III** in toluene at 295 K, the rate constant of S_1-state quenching for the same extra-ligand is essentially higher and amounts to $k_{PET} = 9.9 \cdot 10^8$ s^{-1} (see Table 2). It means that intrinsic quenching mechanism in the last case should be of a different nature with respect to that for triad **I**.

It is seen from Figure 9 that in tetrads **III** and **IV** directly excited S_1-state (Lig...^{1}Dimer*...A) of the dimer $(ZnOEP)_2Ph$

may be deactivated due to the following non-radiative processes: 1A) one-step PET (Lig...^{1}Dimer*...A) $\xrightarrow{k_9}$ (Lig...Dimer$^+$...A$^-$) with rate constant $k_9 = 0.66 \cdot 10^{10}$ s^{-1} for Pim and $k_9 = 2.86 \cdot 10^{10}$ s^{-1} for Q,[34,41] 2A) one-step PET (Lig...^{1}Dimer*...A) $\xrightarrow{k_6}$ (Lig$^-$...Dimer$^+$...A), and 3A) non-radiative singlet-singlet EM (Lig...^{1}Dimer*...A) $\xrightarrow{k_5}$ (^{1}Lig*...Dimer...A). Processes 2A and 3A have been discussed in previous section. We now like to discuss possible pathways which might cause the observed shortening of the extra-ligand locally excited S_1-states in tetrads **III** and **IV**, taking into account the results on experimental and theoretical studies of the charge transfer[42-46] which have been interpreted in terms of long-distance photoinduced electron transfer mediated by superexchange interactions. As has been outlined in detail,[43,44,46] superexchange PET occurs because of coherent mixing of the three or more states of the system. In tetrads **III** and **IV** these states are as follows (Figure 9):[34,41] $|D^*BA\rangle$ corresponds to (^{1}Lig*...Dimer...A), $|D^+B^-A\rangle$ corresponds to the bridge state (Lig$^+$...Dimer$^-$...A) and $|D^+BA^-\rangle$ relates to charge transfer state (Lig$^+$...Dimer...A$^-$). Distant non-overlapping extra-ligand and *A* can exchange their charges through the bridge (dimer), that is a high-lying «spectator» state $|D^+B^-A\rangle$ mediates PET from a donor state $|D^*BA\rangle$ to CT state $|D^+BA^-\rangle$. The estimated energies $E_{D^+B^-A}$ of mediating bridge level in toluene at 295 K for triads **III** and **IV** are presented in Table 2.

It follows from in Figure 9 that the extra-ligand S_1-state (^{1}Lig*...Dimer...A) could arise from both direct photoexcitation and fast (<10 ps) exothermic
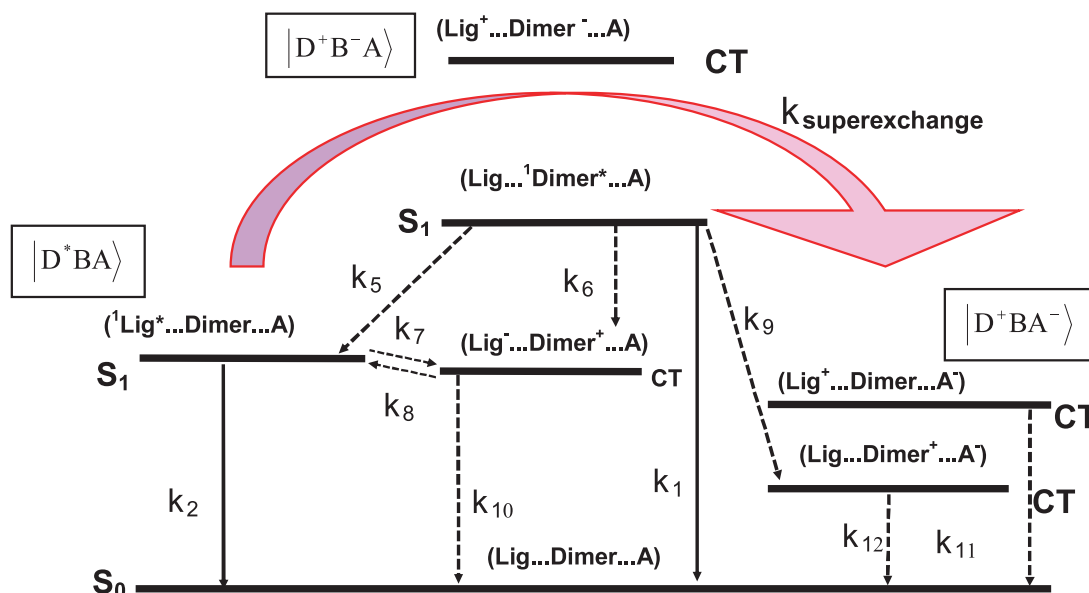
Figure 9. Schematic energy level diagram of excited states for triads with electron acceptor (toluene, 295 K). Indicated are rate constants of deactivation processes partly described in caption to Figure 5 and discussed in the text.

EM process (Lig...^{1}Dimer...A)→(^{1}Lig*... Dimer...A) or via thermally activated charge recombination (Lig$^-$...Dimer$^+$...A) $\xrightarrow{k_8}$ (Dimer...^{1}Lig*...A). Once formed, the excited S$_1$-state of the extra-ligand may decay via two non-radiative processes: 1B) superexchange PET (^{1}Lig*...Dimer...A) $\xrightarrow{k_{superexchange}}$ (Lig$^+$...Dimer...A$^-$), where (ZnOEP)$_2$Ph is a bridge; 2B) photoinduced hole transfer (^{1}Lig*...Dimer...A) $\xrightarrow{k_7}$ (Lig$^-$...Dimer$^+$...A). Being not directly populated a high-lying "spectator" state $\left|D^+B^-A\right\rangle$ mediates the distant PET from a donor state $\left|D^*BA\right\rangle$ to CT state $\left|D^+BA^-\right\rangle$. At last, it should be mentioned that hole transfer pathway 2B) rate constant k$_7$ leads to the formation of CT state (Lig$^-$...Dimer$^+$) which is not a final CT state in *A*-containing triads. Indeed, both ET processes to low-lying CT states, (Lig$^-$...Dimer$^+$...A)→(Lig...Dimer$^+$...A$^-$) and (Lig$^-$...Dimer$^+$...A)→(Lig$^+$...Dimer...A$^-$), may be considered as superexchange PET processes mediated by coherent mixing of the corresponding upper lying CT states.

Thus, self-organised nanoscale porphyrin tetrads containing additional electron acceptors of non-porphyrin nature show complex energy and electron transfer dynamics depending on the geometry of the complex, redox and photophysical properties of interacting subunits as well as on the solvent polarity. The non-radiative deactivation of locally excited S-states in the tetrads includes multistep PET processes of various type (sequential PET, hole transfer and long-range superexchange PET to *A*) thus mimicking the primary charge separation *in vivo*.

Exciton Relaxation and Electron Wave Function Tunneling in Nanocomposites "CdSe/ZnS Quantum Dot-Porphyrin"

Figure 10 shows typical transformations of absorption and photoluminescence (PL) spectra of the QD solution as a function of added monomeric tetra-*meso*-pyridyl substituted porphyrins H$_2$P(m-Pyr)$_4$ at well defined molar ratios $x = $ [H$_2$P] /[QD]. It is seen that upon molar ratio x increase, besides QD absorption bands ($\lambda_{max} = 556$ nm) a linear increase of the porphyrin absorption bands takes place. Noteworthy, in all cases QD absorption remains constant, while the PL (at $\lambda_{max} = 585$ nm for RQD) is considerably quenched upon titration by H$_2$P(Pyr)$_4$ molecules. Time-resolved PL measurements show that emission of pure QD without porphyrin ligand is characterized by a non-exponential decay (Figure 11). The interaction with anchored porphyrin
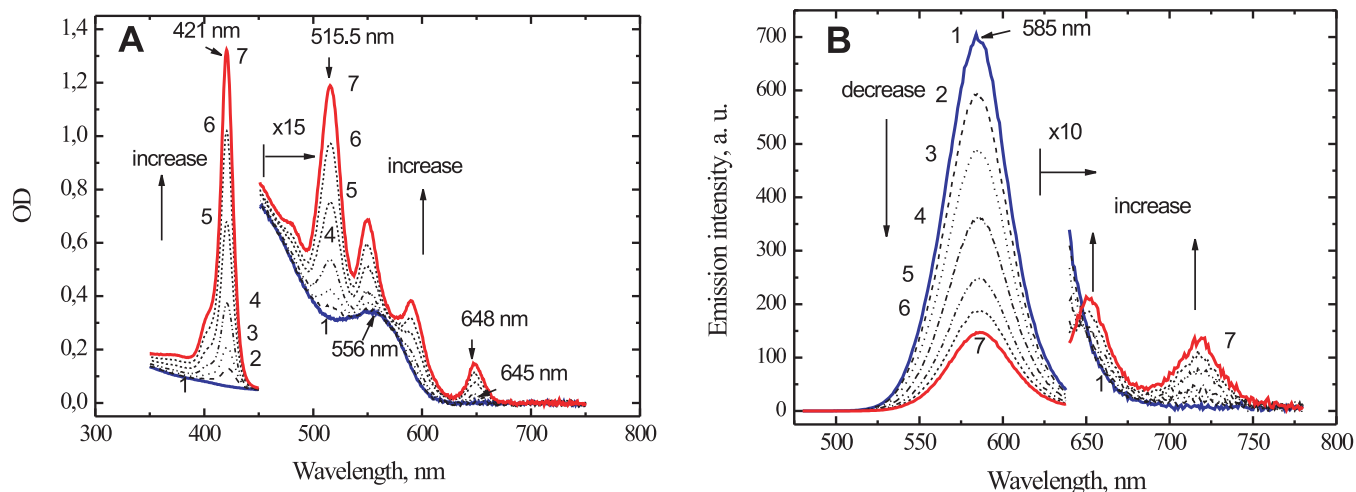

Figure 10. Absorption (A) and emission (B, $\lambda_{ex} = 465$ nm) spectra of CdSe/ZnS QD (diameter of CdSe core d=3.8 nm, 3 ZnS monolayers) and H$_2$P(m-Pyr)$_4$ molecules in toluene at 295 upon molar ratio x increase: 0.0(1); 1.15 (2); 2.3 (3); 4.5 (4); 9.1 (5); 13.5 (6); 17.8 (7).
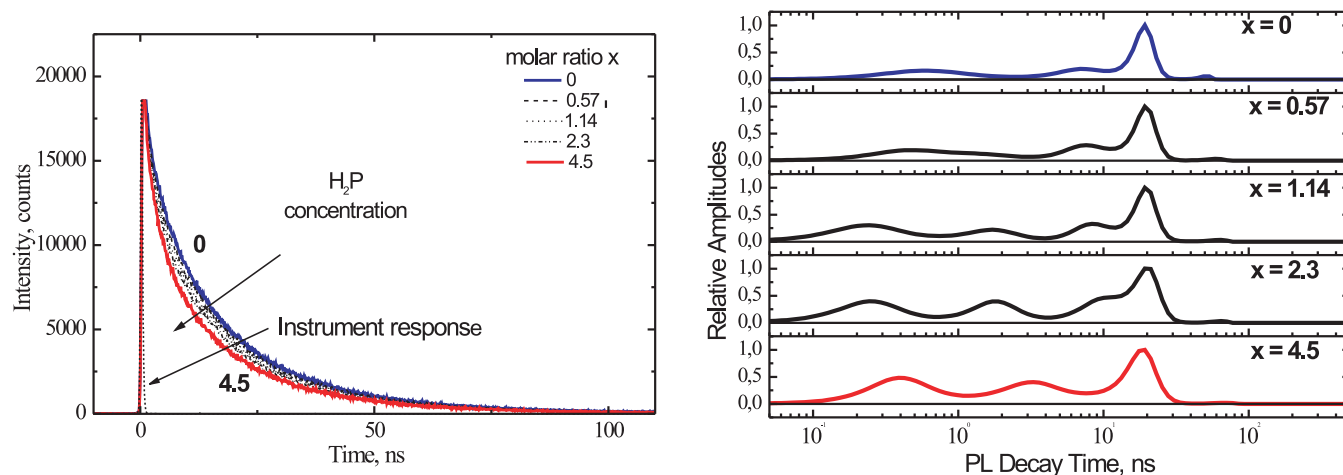

Figure 11. Time-resolved PL traces and decay amplitude distributions for CdSe/ZnS QD (diameter of CdSe core d=3.8 nm, 3 ZnS monolayers) upon molar ratio x increase of H$_2$P-(m-Pyr)$_3$ in toluene (295 K, $\lambda_{exc} = 575$ nm, $\lambda_{em} = 585$ nm).

molecules manifests itself in the appearance and rise of two additional short time components (~ 7 ns and ~ 700 ps).

All these facts indicate that in "QD-monomeric porphyrin" nanosize composites PL quenching of CdSe counterpart is a dynamic process caused by the increased non-radiative relaxation channels in the exited states of a nanocrystal. The increase of the solvent polarity (an addition of 32 vol% of polar acetone to toluene) enhances an additional decrease of QD PL by more than one order of magnitude.[19] In this respect, it should be mentioned that in most cases the formation of QD-dye composites is followed by QD PL quenching which is commonly interpreted as being due to photoinduced charge transfer (CT)[47,48] and/or Foerster-type resonant excitation energy migration (EM) QD→dye.[49,50] Though in most cases ample qualitative evidence for the presence of such quenching processes is given, only a few reports unravel quantitatively, that the PL quenching can uniquely be assigned to CT and/or EM.[49] In fact, PL quenching is may be induced by other processes than EM, which might be related to the inherent photoinduced blinking of single QDs, which has been for the first time described systematically as being due to photoinduced self-trapping of charges in the dielectric medium of the environment of QDs.[51]

Usually in the EM case, the direct verification of the energy migration process as a real reason of PL quenching is the comparison of the experimental values of EM efficiencies via the donor (QD) PL quenching and the sensibilization of the acceptor (porphyrin) fluorescence. Such a comparison has been carried out recently by us for "QD-porphyrin" composites.[19,52] Firstly, it has been definitely shown that the porphyrin fluorescence enhancement is of order of 10% being much smaller as compared to the corresponding quenching efficiency values found from QD photoluminescence. Secondly, in the case of one type of CdSe/ZnS QD (d=2.6 nm and 2 ZnS monolayers), upon the replacement of $H_2P(m-Pyr)_4$ molecules by $CuP(m-Pyr)_4$ and tetrahydroporphyrin, $THP(m-Pyr)_4$ derivatives (thus changing the overlap integral $J(\nu) = \int_0^\infty f_D(\nu)\varepsilon_A(\nu)\frac{d\nu}{\nu^4}$ values by factor of 2.5) the quenching efficiency of QD

photoluminescence remains nearly the same.[20,53] So, the contribution of EM QD→porphyrin to the total PL quenching seems to be minor and hence is negligible in most cases.

Taking into account the results discussed in previous sections, one should conclude that in the case of the photoinduced charge (hole or electron) transfer processes in "QD-porphyrin" composites the porphyrin ligand fluorescence should be also diminished. Nevertheless, fluorescence parameters (efficiency φ_F and decay τ) for $H_2P(m-Pyr)_4$ molecules upon complexation with QDs remain the same practically with respect to those measured for individual ligands and the same conditions.[19,53] In addition, the comparative titrations of the same QD solutions by $H_2P(m-Pyr)_4$ and $THP(m-Pyr)_4$ (holes acceptor) ligands as well as by $H_2P(m^\wedge Pyr)_2(Ph)_2$ and electron acceptors, $H_2P(m^\wedge Pyr)_2(5FPh)_2$ or $H_2P(m^\wedge Pyr)_2(Anthraquinone)_2$, gives the same curves for QD photoluminescence quenching.[19,53] Thus, non-dependence of QD PL quenching efficiency on redox properties of porphyrin ligands and the absence of the porphyrin fluorescence quenching in "QD-porphyrin" composites rules out the dominant role of usual photoinduced charge transfer processes with participation of molecular orbitals of porphyrin macrocycle in QD PL quenching for the systems under study.

We have shown in recent experiments that a third mechanism clearly distinct from CT or EM may cause ligand-induced PL quenching (the so-called non-FRET[52]). This process has not been considered in most of the related publications and is connected with the extension of the wave function of the exciton to the outside of the QD. In this study, the experimental background was the comparative analysis of the photoluminescence quenching by one type of porphyrin $H_2P(m-Pyr)_4$ molecule for QDs of different sizes (as well as having different but known number of ZnS monolayers).

It is seen from Figure 12 that at the same molar ratios x the PL quenching is more effective for smaller QDs. For the analysis of the PL quenching curves as a function of x, Stern-Volmer formalism has been modified as follows

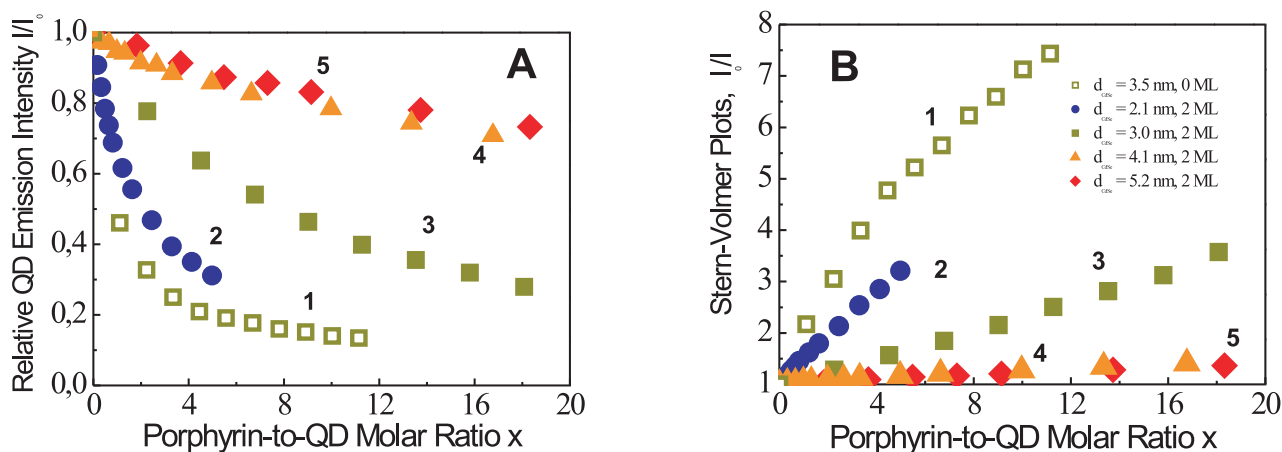$$\frac{I_0}{I} = 1 + \int_0^\infty K(x) \cdot dx, \qquad (2)$$

Figure 12. Relative integrated PL emission intensities $I(x)/I_0$ (A) and Stern-Volmer plots $I_0/I(x)$ (B) for one uncapped (open markers) and four ZnS-capped (solid markers) CdSe/ZnS QDs of various sizes upon titration by $H_2P(m-Pyr)_4$ as function of the molar ratio $x = [H_2P(m-Pyr)_4]/[QD]$ in toluene at 295 K: 1 (□) - d_{CdSe}=3.5 nm/0 monolayers of ZnS; 2 (●) - d_{CdSe}=2.1 nm/2 ML ZnS; 3 (■) - d_{CdSe}=3.0 nm/2 ML ZnS, 4 (▲) - d_{CdSe}=4.1 nm/2 ML ZnS; 5 (◆) -d_{CdSe}=5.2 nm/2 ML ZnS.

where I and I_0 represent QD PL in presence (I) and absence (I_0) of $H_2P(m-Pyr)_4$, respectively. Stern-Volmer parameter $K(x) = \langle K_{SV}(x) \rangle$ is expressed by the first derivative of the experimental data I_0/I as the result of few experimental titration curves for QD of every size. Quenching rate constants k_q are determined by $k_q = K(x)/\tau_0$ and collected in Table 3, where τ_0 is mean intrinsic (non-exponential) PL lifetime measured for every QD.

Data presented in Table 3 show that for CdSe/ZnS quantum dots with two ZnS monolayers k_q values follow a monotonous function drastically decaying with the QD core diameter. From the physico-chemical point of view, we conjecture that upon interaction of $H_2P(m-Pyr)_4$ molecule with QD surface, the electron wave function may be locally modified (via inductive and/or mesomeric effects[53]) forming a surface local state capable to trap the electron of the photogenerated exciton. The general scheme of our model is shown in Figure 13A. We consider the behaviour of the electron wave function at the interface to the functional pyridyl group of the attached porphyrin. The single-carrier envelope wave functions ψ_a in a spherical core/shell QD are determined by the Schrödinger equation

$$\left(\frac{\hbar^2}{2} \frac{\partial^2}{\partial r^2} \left(\frac{1}{m_a^*(r)} + V_a(r) \right) \right) \psi_a = E_a \psi_a, \tag{3}$$

where the index $a = e, h$ represents electron and hole, respectively. Solutions were obtained by applying continuity relations for the single-carrier wave functions at the interfaces between the CdSe core ($i=1$), ZnS shell ($i,j=2$), and matrix ($j=2$), respectively, by assuming that

$$\psi_i(r_{ji}) = \psi_j(r_{ji})$$

and

$$\left. \frac{1}{m_j^*} \frac{d}{dr} \psi_i(r) \right|_{r=r_{ji}} = \left. \frac{1}{m_j^*} \frac{d}{dr} \psi_j(r) \right|_{r=r_{ji}} \tag{4}$$

The comparison of rate constants k_q (points with bars) and the calculated (and scaled) probability densities $\psi^2(r)$ (lines) shows a good correlation. Thus, one point-like charge density perturbation caused by organic linker group or chromophore at QD interface forces the electron of the delocalized exciton of quantum dot to become localized. These results reveal also that single functionalized porphyrin molecules can be considered as one of the probes for the complex interface physics and dynamics of colloidal semiconductor quantum dots.

Interaction of CdSe/ZnS Quantum Dots with Multiporphyrin Complexes

Typically, QD-porphyrin interaction is governed by the Poisson distribution at a given molar ratio x and should be described by finite complexation constant K_C. It follows from the detailed spectral observations[19,20] that at low molar ratios $x = [H_2P]/[QD]$ all $H_2P(Pyr)_n$ molecules especially those with 4 pyridyl rings should be attached to

Table 3. Photoluminescence quenching rate constants k_q for QDs of various CdSe core diameters d_{CdSe} upon titration by $H_2P(m-Pyr)_4$ (toluene, 295 K). Number of ZnS monolayers is n = 2 for all QDs.

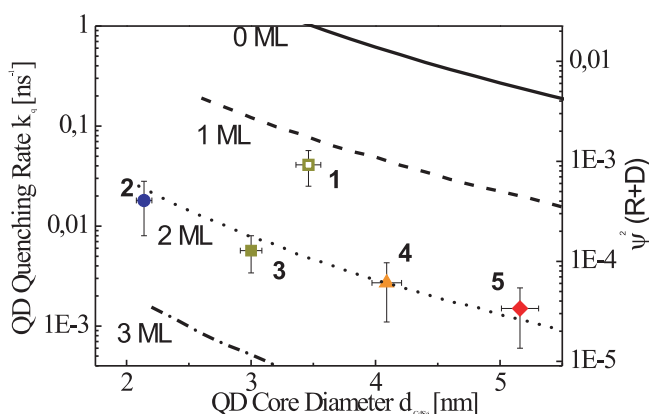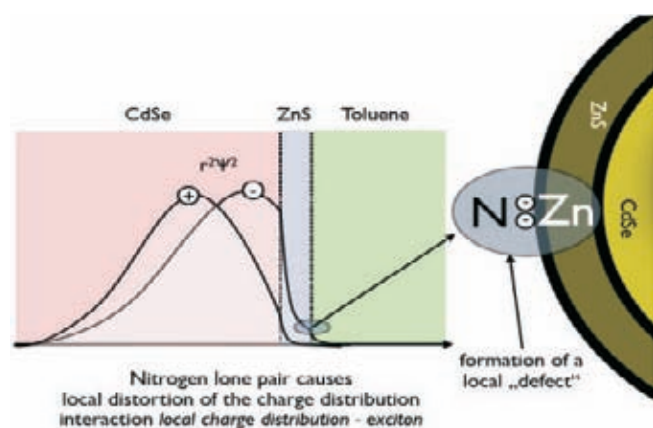| d_{CdSe}, nm	4.3	5.2	6.3	7.3
$\langle K_{SV}(x) \rangle$	0.65±0.10	0.115±0.015	0.055±0.007	0.020±0.003
k_q, ns^{-1}	0.041 ± 0.016	0.0057 ± 0.0023	0.0027 ± 0.0016	0.0015 ± 0.0009

Figure 13. (A) Scheme of the PL quenching model: upon excitation, an electron-hole pair (exciton is created in the CdSe core of the QD). The electron is delocalized over the core and the ZnS shell. As a result of the finite ZnS energy barrier E_{ZnS}, the electron can tunnel to the ZnS surface (and the environment). Due to the presence of pyridyl coordinated porphyrin molecule, the electron becomes partly localized in a volume element in the vicinity of the attachment site, described by the $\psi^2(r)$. (B) Comparison of the experimentally determined quenching rate constants k_q (left axis) and calculated size-dependent curves (right axis) for the probability density functions $\psi^2(r=R+D)$ of a $1s$ electron at the outer interface ($r=R+D$) between the ZnS shell and the environment for various ZnS shell thicknesses D. The constant C in equation $k_q(r) = C\psi^2(r)$ has been adjusted with respect to $\psi^2(R+D)$ to fit the experimental value at $d_{CdSe}=4.1$ nm/2 ML ZnS (point 4). QD parameters are the same as in Figure 12.

the CdSe/ZnS surface. In addition, since the noticeable QD photoluminescence quenching is observed at molar ratios $x < 1$ even (see quenching curves in Figure 12A), one can neglect (following statistical arguments) nanoassemblies with more than one ligand per QD. We thus can discuss the experimental titration data on the basis of a bi-molecular reaction scheme valid for a dynamic equilibrium between complexed and free constituents as has been usually applied in numerous experiments on the formation of multiporphyrin assemblies[6,27,28] and discussed in previous sections. Following this idea and using equation (1) where I/I_0 corresponds to QD photoluminescence quenching as a function of the molar ratio x, the values of the complexation constant K_c have been estimated for solutions CdSe/ZnS quantum dots (d_{CdSe}=2.5 nm and 2 ZnS multilayers, C_{QD} = 5·10⁻⁸ M, toluene, 295 K) as a function of various $H_2P(Pyr)_n$ extra-ligands[20] (see Table 4).

Table 4. Complexation constants K_c for composites based on CdSe/ZnS quantum dots (d_{CdSe}=2.5 nm, 2 ZnS multilayers) and $H_2P(Pyr)_n$ extra-ligands with n = 1, 2, 3 and 4, calculated using equation (1).

Extra-ligand	K_C, 10⁷ M⁻¹
H_2P (m-Pyr)$_1$	<0.015
H_2P (m^Pyr)$_2$	0.34
H_2P (m-Pyr)$_3$	0.78
H_2P (m-Pyr)$_4$	2.6

Data of Table 4 clearly show that K_c values are increased with the number of pyridyl rings thus reflecting a dynamic equilibrium between QD and $H_2P(Pyr)_n$. Comparing K_C values for "QD-porphyrin" composites with those obtained for various multiporphyrin complexes[6] (presented in experimental section) shows that with respect to two-fold extra-coordination they are in a comparable range but being much larger as compared to one-fold coordination. It should be mentioned also that the formation of "QD-porphyrin" composites is due to the independent multipoint interaction and relative K_C values are determined by statistical factors,
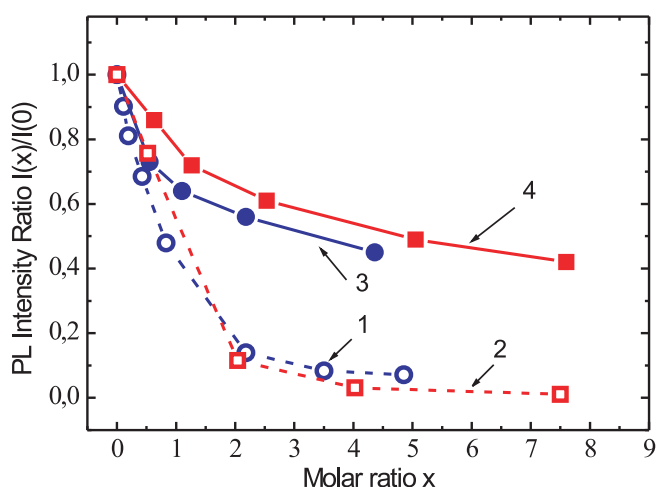
while for self-assembled porphyrin triads, tetrads and pentads allosteric effects play a dominant role.[6]

The direct titration of QD solutions by porphyrin triads $(ZnOEP)_2Ph\otimes H_2P(m\text{-}Pyr)_3$ and pentads $2(ZnOEP)_2Ph\otimes H_2P(m\text{-}Pyr)_4$ gives an additional information that proofs the above conclusion on K_C values for "QD-porphyrin" composites. Indeed, comparative experiments have shown (Figure 14) that upon titration of QD solution by triads or pentads, PL quenching for CdSe/ZnS quantum dots is relatively smaller with respect to the quenching by monomeric porphyrins (the same ones as included in triad or pentad). It is seen from Figure 14 that the titration curves for the triad and pentad are rather close, and at molar ratios $x > 2$ the experimental quenching values $I(x)/I(0)$ in these cases are higher by ~2 times in comparison with those measured for individual porphyrin molecules $H_2P(m\text{-}Pyr)_3$ and $H_2P(m\text{-}Pyr)_4$ at the same molar ratios x. Really, in the solutions containing QD and triad/pentad there is a dynamic competition between QD and the dimer $(ZnOEP)_2Ph$ to complex with the porphyrin extra-ligand. In this case statistically, if complexation constants K_C are comparable for "QD-porphyrin" composites and triads (K_C =1.5·10⁷ M⁻¹)⁶ or pentads (K_C =1.6·10⁷ M⁻¹)⁶, the QD PL quenching values $I(x)/I(0)$ should be smaller by ~2 times compare to the corresponding values obtained for the titration of the same QD by individual porphyrin extra-ligands.

In addition, at every titration step we have measured the relative quantum yields of the extra-ligand
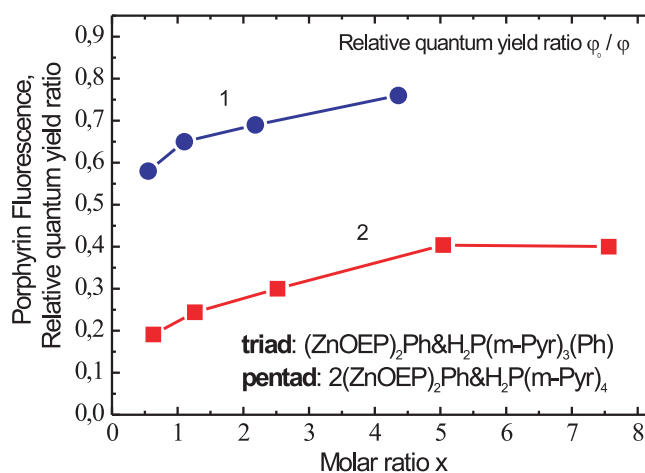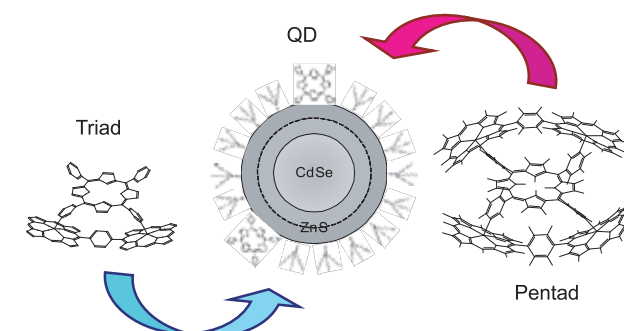

Figure 14. PL quenching for CdSe/ZnS quantum dots (d_{CdSe}=2.5 nm, 2 ZnS multilayers) upon titration by individual porphyrin molecules $H_2P(m\text{-}Pyr)_3$ (1) and $H_2P(m\text{-}Pyr)_4$ (2), as well as by triads $(ZnOEP)_2Ph\otimes H_2P(m\text{-}Pyr)_3$ (3) and pentads $2(ZnOEP)_2Ph\otimes H_2P(m\text{-}Pyr)_4$ (4) in toluene at 295 K (λ_{ex} = 465 nm, λ_{rec} = 523 nm).

Figure 15. Relative quantum yield ratio of porphyrin fluorescence in pure triad (1) and pentad (2) solutions with respect to the same solutions containing the constant concentration of CdSe/ZnS quantum dots (d_{CdSe}=2.5 nm, 2 ZnS multilayers, C = 3.4·10⁻⁷ M) upon the increase of the molar ratio of triads and pentads (toluene, 295 K, λ_{ex} = 545 nm, λ_{rec} = 718 nm - porphyrin emission band).

fluorescence in individual triad and pentad solutions (φ_0), and the corresponding values φ for the same porphyrin subunits in comparative solutions containing the constant QD concentration and the same molar ratios of triads and pentads, respectively. It is seen from Figure 15 that at low molar ratios x = [triad]/[QD] and [pentad]/[QD] the relative values φ_0/φ are smaller being increased upon rising x. It means that at low molar ratios x the relative quantum yields of the porphyrin in triad and pentad solutions are smaller with respect to those measured for the same solutions additionally containing QD. In the later case, the part of porphyrin molecules is anchored on QD surface (and is not quenched, as discussed above) thus manifesting in the relative rise of the porphyrin fluorescence efficiency with respect to the pure triad and pentad solutions (where porphyrin molecules do show the emission quenching due to a hole transfer[6,34,36,37]). At $x > 2$ the observed difference between φ_0 and φ values becomes smaller with noticeable saturation effect. Really, in the case of limited number of "vacancies" on the QD surface capable to attach porphyrin ligands, the rise of x ratio leads to the increase of porphyrin molecules uncomplexed with QDs but still ready to interact with the dimer (ZnOEP)$_2$Ph thus resulting in the rise of the triads and pentads in the solution. The difference between curves 1 and 2 reflects the fact that porphyrin fluorescence quenching is stronger in pentads compare to triads.[6,34]

At last, our preliminary results have shown that a supramolecular approach based on the non-covalent two-fold extra-ligation can be successfully employed to create nanosize heterocomposites containing QD and multiporphyrin complexes. In these experiments, CdSe/ZnS quantum dots (d_{CdSe}=1.9 nm, 2 ZnS multilayers) the extra-ligand H$_2$P(p-Pyr)$_4$ have been chosen due to the following reasons. 1) Upon interaction with porphyrin molecules, QD PL quenching is the most pronounced for smaller nanocrystals,[19,52] and thus we used the smallest ones.
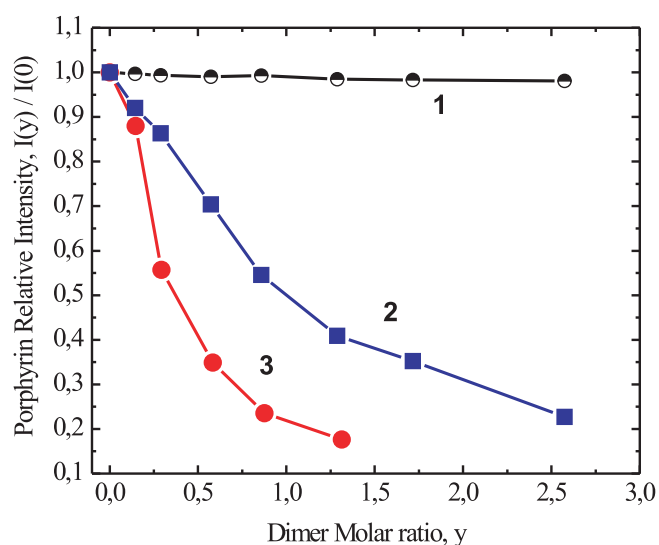
2) In the case of H$_2$P(p-Pyr)$_4$ molecule, *para*-nitrogens of the two outer pyridyl rings (the other two are attached to QD surface) should be a little bit above neighboring TOPO molecules, so steric interactions of these TOPO molecules with an additional appropriate porphyrin subunit seem to be diminished significantly. Correspondingly, it opens a possibility for the dimer subunit (ZnOEP)$_2$Ph to be connected with H$_2$P(p-Pyr)$_4$ extra-ligand via two outer *para*-nitrogens of the later one.

Following the idea[20] that at low molar ratios x all (Pyr)$_n$H$_2$P molecules especially those with 4 pyridyl rings should be attached to the CdSe/ZnS surface, for further experiments we have prepared the mixture solution of QD and H$_2$P(p-Pyr)$_4$ at x=0.45 where QD PL quenching is still well defined $I(x)/I(0)$ = 0.6 and all porphyrin molecules are anchored on QD surface Then, this initial mixture solution have been titrated by the dimer (ZnOEP)$_2$Ph. For comparison, the same titration procedure by this dimer has been carried out for the solution containing individual H$_2$P(p-Pyr)$_4$ molecules at the same initial concentration. By this way we have comparatively examined what happens in solutions with and without QDs. The detailed spectral picture and the analysis of the obtained results will be presented in our forthcoming paper. Here, we outline the main findings indicating that the formation of nanosize heterocomposites containing QD and multiporphyrin complexes is possible. Fig. 16 shows that the addition of increasing amounts of the dimer (ZnOEP)$_2$Ph to the mixture solution [QD + H$_2$P(p-Pyr)$_4$] does not lead to the decrease of QD PL relative intensity (curve 1). We attribute this observation to the fact that the quenching counterpart of the "QD-porphyrin" composites (namely, H$_2$P(p-Pyr)$_4$) is still attached to QD upon addition of the dimer. On the other hand, it is seen that the fluorescence of anchored H$_2$P(p-Pyr)$_4$ ligand is continuously quenched upon titration by the dimer (curve 2). Noteworthy, the comparative titration experiments for solution containing individual molecules H$_2$P(p-Pyr)$_4$ at the same concentration like being used in the initial mixture solution [QD + H$_2$P(p-Pyr)$_4$], show also H$_2$P(p-Pyr)$_4$ fluorescence quenching (curve 3). The last quenching is caused be pentads formation (where H$_2$P(p-Pyr)$_4$ fluorescence is quenched[6,28,54]) and is noticeably stronger with respect to a mixture solution (curve 2).

These results may be explained as follows. Being anchored to QD surface via two (p-Pyr) rings, the ligand H$_2$P(p-Pyr)$_4$ may attach the dimer (ZnOEP)$_2$Ph by the coordination of the dimer two central Zn ions with *para*-nitrogens of two outer (p-Pyr) rings of the ligand (Figure 17). This complexation seems to be favourable because of weakening of steric interactions of the dimer with neighboring TOPO molecules in the H$_2$P(p-Pyr)$_4$ case. In the result, the triad (ZnOEP)$_2$⊗(p-Pyr)$_4$H$_2$P should be formed on QD surface. Moreover, according to our data[6,28,54] the H$_2$P(p-Pyr)$_4$ fluorescence in the triad should be less quenched with respect to the same extra-ligand emission in the pentad. It explains the observed fluorescence smaller quenching for H$_2$P(p-Pyr)$_4$ found in mixture [QD + H$_2$P(p-Pyr)$_4$] solution (curve 2, triad formation on QD surface) in comparison with individual H$_2$P(p-Pyr)$_4$ solution (curve 3, usual pentad formation in a solution) at the same relative concentrations of the dimer.

Figure 16. QD photoluminescence (1, λ_{rec} = 481 nm) and extra-ligand H$_2$P(p-Pyr)$_4$ fluorescence (2, 3, λ_{rec} = 714 nm) relative intensities, $I(x)/I(0)$, as a function of the dimer (ZnOEP)$_2$Ph molar ratio y for mixture [QD + (p-Pyr)$_4$H$_2$P, x = 0.45] solution (1 and 2) and for individual ligand H$_2$P(p-Pyr)$_4$ (3). Toluene, 295K, λ_{ex} = 465 nm.
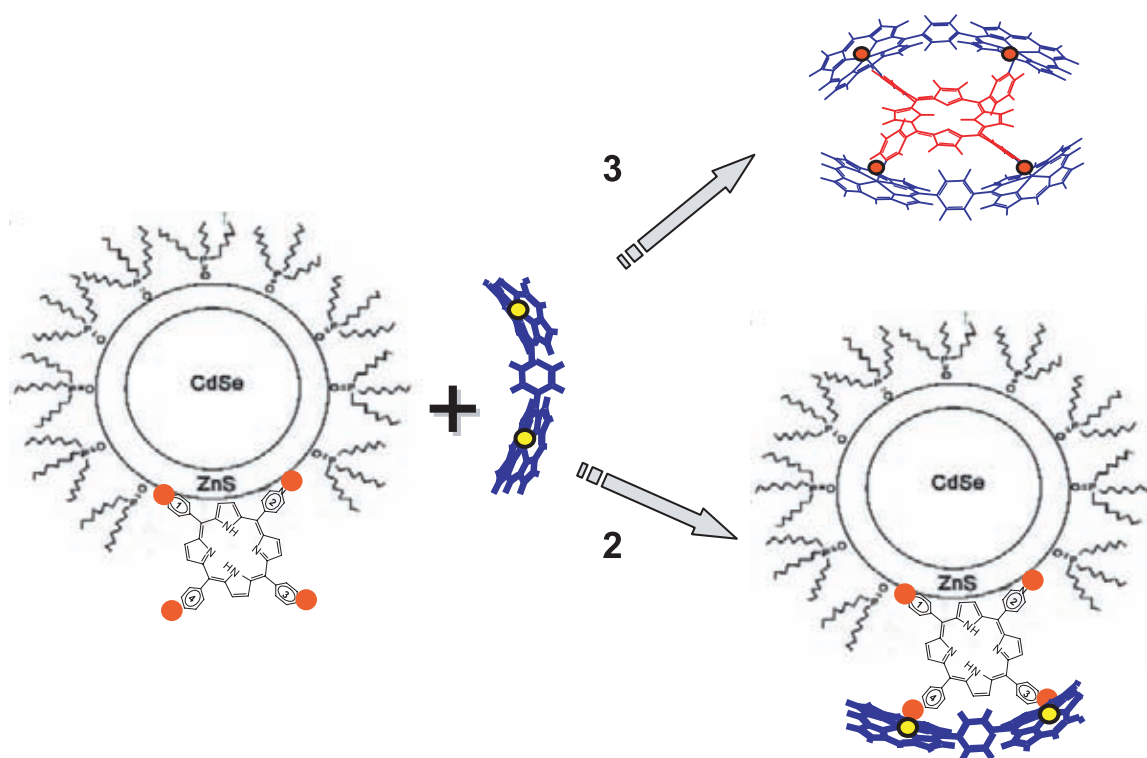
Figure 17. Scheme of competitive formation processes for "QD-porphyrin triad" composites (2) and self-organized pentads (3).

Conclusions

Here, we demonstrated that by means of a non-covalent two-fold extra-ligation in conjunction with Zn-porphyrin chemical dimers it is possible to create by predictable manner a variety of multiporphyrin structures that are capable of undergoing photodriven fast effective intra-complex energy migration and photoinduced charge separation. The cooperative existence and competition between PET and EM depends on the temperature and polarity of surrounding and results in a complex relaxation dynamics of the locally excited S_1- and T_1-states of interacting counterparts.

In addition, self-assembly principles (based on the non-covalent two-fold extra-ligation) elaborated for the formation of porphyrin triads and pentads may be successfully extended to anchor in a systematic and directed way π-conjugated tetrapyrrole molecules on semiconductor CdSe/ZnS quantum dot surfaces in solutions. With respect to two-fold extra-coordination, complexation constant K_C values for "QD-porphyrin" composites are in a comparable range with those obtained for various multiporphyrin complexes. Depending on CdSe size (optical tunability), ZnS layer thickness, spectral and anchoring properties of porphyrin moieties (chemical tunability), the photoluminescence quenching for quantum dots in "QD-porphyrin" composites with closely contacting organic and inorganic components can be understood in terms of a tunnelling of the electron (of the excited electron-hole pair) followed by a (self-)localization of the electron or formation of trap states.

Our preliminary results have shown also that the above supramolecular approach can be successfully employed to create nanosize heterocomposites consisting of CdSe/ZnS QDs with multichromophore organic component (poprhyrin triads) anchored on QD surface. The presented results show that design and self-assembly of organic/inorganic moieties into functional superstructures with vectorial relaxation are perspective for nanotechnology and supramolecular electronics.

References

1. *An Introduction to Molecular Electronics* (Petty M.C., Bryce M.R., Bloor D., Eds.) London, Melbourne, Auckland: Edward Arnold, a division of Holder Headline PLC, **1995**. 320 p.
2. Mansoori G. Ali. *Principles of Nanotechnology. Molecular-Based Study of Condensed Matter in Small Systems*. Chicago: University of Illinois at Chicago, USA, **2005**.
3. *The Reaction Center of Photosynthetic Bacteria. Structure and Dynamics* (Michel-Beyerle M.-E., Ed.) Berlin-Heidelberg: Springer-Verlag, **1996**.
4. Balzani V., Scandola F. *Supramolecular Photochemistry*. New York, London, Toronto, Sydney, Tokyo, Singapore: Ellis Horwoord, **1991**.
5. Liu Z., Yasseri A.A., Lindsey J.S., Bocian D.F. *Science* **2003**, *302*, 1543-1544.
6. Zenkevich E.I., von Borczyskowski C. *Multiporphyrin Self-assembled Arrays in Solutions and Films: Thermodynamics, Spectroscopy and Photochemistry*/ in Handbook of Polyelectrolytes and Their Applications (Tripathy S.K., Kumar J., Nalwa H.S., Eds.) USA: American Scientific Publishers, **2002**, 2, Ch. 11, 301-348.

7. Peng X., Aratani N., Takagi A., Matsumoto T., Kawai T., Hwang I.-W., Ahn T.K., Osuka A. *J. Amer. Chem. Soc.* **2004**, *126*, 4468-4469.

8. Imahori H. *J. Phys. Chem. B* **2004**, *108*, 6130-6143.

9. Ogawa K., Hara C., Kobuke Y. *J. Porphyrins Phthalocyanines* **2007**, *11*, 359-365.

10. Sandanayaka A.S.D., Araki Y., Wada T., Hasobe T. *J. Phys. Chem. C* **2008**, *112*, 19209–19216.

11. Efros A.L., Rosen M. *Ann. Rev. of Material Sci.* **2000**, *30*, 475-521.

12. Gaponenko S.V. *Optical Properties of Semiconductor Nanocrystals*. Cambridge: University Press, **1998**.

13. Klimov V. *Optical Properties of Nanocrystals*/ in Handbook of Nanostructured Materials and Nanotechnology (Nalwa H.S., Ed.) USA: Acad. Press **2000**, Vol. 4, 451-527.

14. *Semiconductor Nanocrystal Quantum Dots (Synthesis, Assembly, Spectroscopy and Applications)* (Rogach A.L., Ed.) Wien: Springer-Verlag **2008**. 369 p.

15. Talapin D.V., Haubold S., Rogach A.L., Kornowski A., Haase M., Weller H. *J. Phys. Chem. B* **2001**, *105*, 2260-2263.

16. *Nanoparticles: From Theory to Applications* (Schmid G., Ed.) Weinheim, Germany: Wiley-VCH, **2004**.

17. Hagfeldt A., Gratzel M. *Acc. Chem. Res.* **2000**, *33*, 269-277.

18. Clapp A. R.. Medintz I. L, Mattoussi H. *ChemPhys Chem*. **2006**, *7*, 47-57.

19. Zenkevich E., Shulga A., Cichos F., Petrov E., Blaudeck T., von Borczyskowski C. *J. Phys. Chem. B.* **2005**, *109*, 8679-8692.

20. Zenkevich E., Blaudeck T., Shulga A., Cichos F., von Borczyskowski C. *J. Luminescence* **2007**, *122*, 784-788.

21. Kilin D.S., Tsemekhman K., Prezhdo O.V., Zenkevich E.I., von Borczyskowski C. *J. Photochem. Phobiol A: Chemistry* **2007**, *190*, 342-354.

22. Dayal S., Lou Y., Samia A.C.S., Berlin J.C., Kenney M.E., Burda C. *J. Am. Chem. Soc.* **2006**, *128*, 13974-13975.

23. Funston A.M., Jasieniak J.J., Mulvaney P. *Adv. Mater.* **2008**, DOI: 10-1002/adma.200703196, 1-7.

24. De M., Ghosh P.S., Rotello V.M. *Adv. Mater.* **2008**, *20*, 1-17.

25. Coe-Sullivan S., Woo W.-K., Steckel J.S., Bawendi M., Bulovic V. *Organic Electronics* **2003**, *4*, 123-130.

26. Katoh R., Furube A., Yoshihara T., Hara K., Fujikashi G., Takano A., Murata S., Arakawa H., Tachiya M. *J. Phys. Chem. B* **2004**, *108*, 4818-4822.

27. Zenkevich E.I., von Borczyskowski C., Shulga A.M. *J. Porphyrins Phthalocyanines* **2003**, *7*, 731-754.

28. Chernook A.V., Shulga A.M., Zenkevich E.I., Rempel U., von Borczyskowski C. *J. Phys. Chem.* **1996**, *100*, 1918-1926.

29. Bachilo S., Willert A., Rempel U., M.Shulga A., Zenkevich E.I., von Borczyskowski C. *J. Photochem. Photobiol. A: Chemistry* **1999**, *126*, 99-112.

30. Zenkevich E.I., Shulga A.M., Bachilo S.M., Rempel U., von Richthofen J., von Borczyskowski C. *J. Luminescence* **1998**, *76-77*, 354-358.

31. Blaudeck T., Zenkevich E., Cichos F., von Borczyskowski C. *J. Phys. Chem. C* **2008**, *112*, 20251–20257.

32. Zenkevich E.I., Blaudeck T., Heidenaetsch M., Cichos F., von Borczyskowski C. *Teoret. i Eksperiment. Khimiya* **2009**, *45*, 17-26. (in Russ.).

33. Sagun E.I., Zenkevich E.I., Knyukshto V.N., Shulga A.M., Starukhin D.A., von Borczyskowski C. *Chemical Physics* **2002**, *275*, 211-237.

34. Zenkevich E.I., von Borczyskowski C., Shulga A.M., Bachilo S.M., Rempel U., Willert A. *Chemical Physics* **2002**, *275*, 185-209.

35. Hsiao J.-S., Krueger B.P., Wagner R.W., Johnson T.E., Delaney J.K., Mauzerall D.C., Fleming G.R., Lindsey J.S., Bocian D.F., Donohoe R. *J. J. Amer. Chem. Soc.* **1996**, *118*, 11181-11189.

36. Zenkevich E.I., Kilin D.S., Willert A., Bachilo S.M., Shulga A.M., Rempel U., von Borczyskowski C. *Molecular Crystals and Liquid Crystals* **2001**, *326*, 83-88.

37. Zenkevich E.I., Willert A., Bachilo S.M., Rempel U., Kilin D.S., Shulga A.M., von Borczyskowski C. *Materials Science and Engineering C* **2001**, *18*, 99-111.

38. Foerster Th. in *Modern Quantum Chemistry*. New York: Acad. Press **1965**, *3*, 93-118.

39. Osuka A., Nakajima S., Maruyama K., Mataga N., Asahi T. *Chemistry Letters* **1991**, 1003-1007.

40. Gust D., Moore T.A., Moore A.L., Leggett L., Lin S., DeGraziano J.M., Hermant R.M., Nicodem D., Craig P., Seely G.R., Nieman R.A. *J. Phys. Chem.* **1993**, *97*, 7926-7933.

41. Zenkevich E.I., Shulga A.M., von Borczyskowski C. *Physica E (Low Dimensional Systems and Nanostructures)* **2002**, *14*, 277-281.

42. Wasielewski M.R., Johnson D.J., Swec W.A., Kersey K.M., Minsek D.W. *J. Am. Chem. Soc.* **1988**, *110*, 7219-7225.

43. Bixon M., Jortner J., Michel-Beyerle M.E. *Chem. Phys.* **1995**, *197*, 389-415.

44. Davis W., Wasielewski M.R., Ratner M., Mujica V., Nitzan A. *J. Phys. Chem.* **1997**, *101*, 6158-6165.

45. Rempel U., Meyer S., von Maltzan B., von Borczyskowski C. *J. Luminescence* **1998**, *78*, 97-103.

46. Schreiber M., Kilin D., Kleinekathofer U. *J. Luminescence* **1999**, *83-84*, 235-240.

47. Schmelz O., Mews A., Basché T., Herrmann A., Müllen K. *Langmuir* **2001**, *17*, 2861-2865.

48. Boulesbaa A., Issac A., Stockwell D., *et. al. J. Amer. Chem. Soc.* **2007**, *129*, 15132-1535.

49. Clapp A. R., Medintz I. L., Mattoussi H. *Chem. Phys.* **2006**, *7*, 47-57.

50. Orlova A.O., Maslov V.G., Baranov A.V., *et. al. Optika i Spektroskopiya* **2008**, *726*, 105-1113. (in Russ.).

51. Issac A., von Borczyskowski C., Cichos F. *Phys. Rev.* **2005**, *B 71*, 16130.

52. Blaudeck T., Zenkevich E., Cichos F., von Borczyskowski C. *J. Phys. Chem. C* **2008**, *112*, 20251–20257.

53. Zenkevich E.I., Sagun E.I., Yarovoi A.A., A.M. Shulga, Knyukshto V.N., Stupak A.P., von Borczyskowski C. *Optika i Spektroskopiya* **2007**, *103*, 998-1009. (in Russ.).

54. Chernook A.V., Rempel U., von Borczyskowski C., Zenkevich E.I., Shulga A. *Chem. Phys. Letters* **1996**, *254*, 229-241.